Marine and Petroleum Geology 139 (2022) 105625

Contents lists available at ScienceDirect

Marine and Petroleum Geology

journal homepage: www.elsevier.com/locate/marpetgeo

Characteristics and formation mechanism of the tight tuff reservoirs of the Upper Triassic Chang 7 member in the southern Ordos Basin, China

Qing Li [a,b,*], Hao Lu [a,b], Jiangshan Li [a,b], Shenghe Wu [a,b], Yue Wu [c], Lang Wen [a,b], Yu He [a,b], Fengqiang Qi [a,b]

[a] State Key Laboratory of Petroleum Resources and Prospecting, Beijing, 102249, China
[b] College of Geosciences, China University of Petroleum, Beijing, 102249, China
[c] Petroleum Exploration and Development Institute of SINOPEC, Beijing, 100083, China

ARTICLE INFO

Keywords:
Devitrification
Volcanic reservoir
Tight oil
Pore evolution
Yanchang formation

ABSTRACT

Organic-rich shales are commonly associated with tuff layers. Previous studies have mainly focused on the influence of water-laid tuffs on the primary productivity and enrichment of organic matter. Tuffs can also act as tight or low permeability reservoirs or as sweet spots in shales. However, the characteristics and formation mechanism of tight tuff reservoirs are poorly explored. The tuffs in the study area are divided into five lithologies: vitric tuff, crystal-vitric tuff, crystal tuff, tuffite, and tuffaceous sandstone. The pores in these tuffs have various types and sizes, and mainly include (1) intergranular pores, (2) intragranular pores, (3) dissolution pores, (4) seams around grains, (5) organic matter related pores, and (6) fractures. The tuffs form tight reservoir rocks with low porosity and permeability, ranging from 2.33% to 12.62% (average 7.2%) and from 0.000518 mD to 0.281mD (average 0.0783 mD), respectively. The average porosity and permeability of the tuffs are better than those of shales, and the pores in the tuff reservoirs are often filled with oil residues, which indicate that the tuff reservoirs may be favorable for oil and gas accumulations.

The tuff reservoir qualities have strong heterogeneity, which are significantly controlled by lithology, grain size, components, devitrification, dissolution, and fluid pathway systems. Tuffs with large grain sizes commonly have high primary porosity with relatively more cracks and seams within and around grains, which can be conducive to the entry of late diagenetic fluids, which cause tuff reservoirs to be more prone to devitrification and dissolution. The devitrification of volcanic glass can produce abundant microcrystalline quartz, feldspars and intergranular pores, and can greatly improve the reservoir quality. Devitrification has generally occurred in the vitric tuffs and crystal-vitric tuffs, and the porosities have a positive covariation with the quartz contents in the two lithologies. The devitrification pores can be further enlarged by dissolution. Devitrification and dissolution were controlled by the tuff compositions and fluid actions. The fluid pathway systems, including scouring surfaces, bedding, fractures, and well-developed primary pores, controlled the fluid movement. Tuffs that contain high volcanic glass contents and coarse particles with abundant beddings and fractures are prone to intense devitrification and dissolution, which results in high reservoir quality.

1. Introduction

Tuffs and tuffaceous sediments have important geological significance, and have attracted extensive attention from researchers in recent years. Volcanic ash deposition, which has an instantaneous and isochronous nature, is commonly widely distributed and has distinctive characteristics in sedimentary basins, which make tuffs good marker beds for stratigraphic correlations (Zhong et al., 1996; Desmastes et al., 2007). The nutrients (such as Fe, P_2O_5, and CaO) released during tuff deposition can promote algae blooms and result in high-quality source rocks in lake basins (Li et al., 2020a; Zhang et al., 2009). Tuffs can also be used to recover the surrounding synchronous tectonic-magmatic geological events (Wang et al., 2017; Yang et al., 2019), to establish the time and development sequences of synchronous geological events

* Corresponding author. State Key Laboratory of Petroleum Resources and Prospecting, College of Geosciences, China University of Petroleum, Beijing, 102249, China.
E-mail address: liqing@cup.edu.cn (Q. Li).

https://doi.org/10.1016/j.marpetgeo.2022.105625
Received 22 November 2021; Received in revised form 21 February 2022; Accepted 1 March 2022
Available online 4 March 2022

(Dong et al., 1997), and to restore paleoenvironments (Lowe, 2011). In addition, tuffs can act as oil and gas reservoirs. Tuff reservoirs have been found worldwide in many oilfields, such as the tuff reservoirs of the Tiaohu Formation in the Santanghu Basin (Xu et al., 2017; Ma et al., 2016), the Upper Permian Formation in the Junggar Basin (Liu et al., 2014), the Lower Cretaceous Alashan Formation in the Erlian Basin (Gao et al., 2006), in the Richland oilfield Monroe uplift of the USA (Zhang et al., 2010). And petroleum has been produced from many tuff reservoirs. For example, high oil product (up to 131 m^3/day per well, well M58H) was gained from tuff reservoir (about 10 m thick) after artificial fracturing in the Tiaohu formation of Permian in the Santanghu Basin (Ma et al., 2015, 2016).

Late Triassic volcanism in the region of the Ordos Basin resulted in deposition of several tuff layers in the Yangchang Formation, including the prominent Chang 7 member. A large number of studies have studied the geochemical characteristics of the tuffs (Lai et al., 2010), the influence of tuff on organic matter enrichment (Li et al., 2020a), and the tuff distribution in the study area (Qiu et al., 2009). The results show that the tuffs in this area are closely related to the Qinling orogenic belt (Wang et al., 2017). The tuffs in the Chang 7_3 member are generally distributed in a northwest direction, and the thickness of the tuff layers gradually thin from southwest to northeast (Qiu et al., 2009). The volcanic ash is interpreted to have promoted primary organic productivity and organic matter enrichment during the depositional period of the Chang 7 member (Li et al., 2020a).

The tuff reservoir in the Chang 7 member in the Ordos Basin is commonly oil-bearing, indicating that other tuffs may also have large exploration potential as important unconventional oil and gas reservoirs. The tuffs in the study area are heterogeneous; exhibiting a wide range of reservoir quality. Exploration for tuff reservoirs in the Ordos Basin has been limited because the controls of reservoir quality are poorly understood.

The purpose of this study is to better characterize the reservoir properties of the Chang 7 tuff member and the significant controls on reservoir quality that may also serve as a model for the exploration and development of tuff reservoirs in the Ordos and other basins.

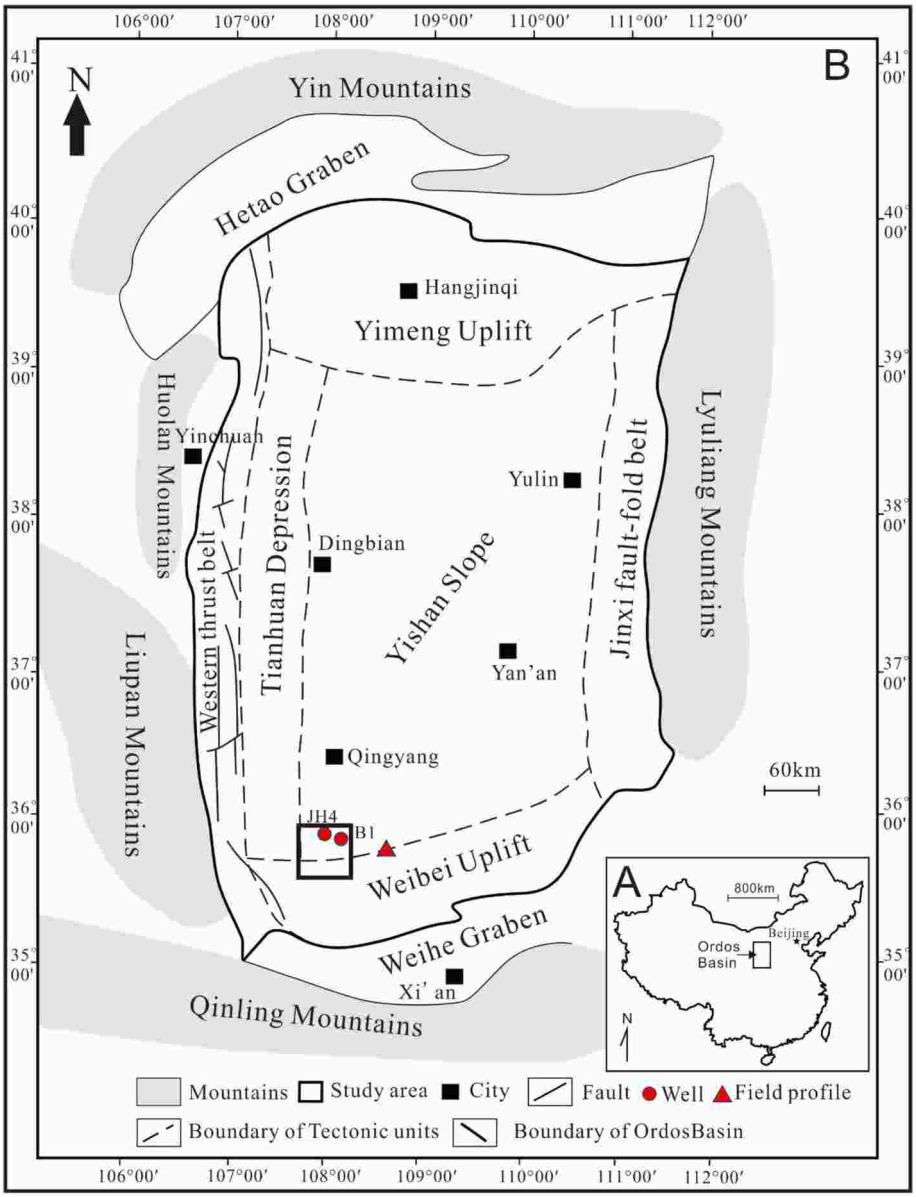

Fig. 1. (A) Location of the Ordos Basin in China. (B) Geological background of the Ordos Basin, together with the study area and sampling well locations (modified after Lyu et al., 2017).

2. Geological setting

The Ordos Basin is the second largest sedimentary basin in China, located in the central part of China (Fig. 1A), with an approximately area of 320, 000 km^2 (He et al., 2016; Xian et al., 2018; Li et al., 2020a). The Ordos Basin can be divided into six tectonic units (Xian et al., 2018): the Yimeng uplift in the north, Weibei uplift in the south, Jinxi fold belt in the east, Tianhuan depression and thrust belt in the west, and the expansive Yishan slope in the center (Fig. 1B). The Ordos Basin has undergone multiple evolutionary stages: Early Paleozoic marginal ocean basin, Early to Late Paleozoic littoral basin, Late Permian to Middle Triassic large interior basin, and Late Triassic to Early Cretaceous paraforeland basin (Wang et al., 2017). During the Late Triassic Period, the North China Plate collided with and was integrated with the Yangtze Plate, which are called Qinling orogenesis (Zhang et al., 2017). As a result of the Indosinian orogeny and Qingling orogenies, the southern Ordos Basin evolved into a terrestrial lacustrine basin and developed a fluvial-lacustrine sedimentary system in the Upper Triassic Yanchang Formation (Qiu et al., 2015a,b).

The Upper Triassic Yanchang Formation is further subdivided by its sedimentary cycles and lithological assemblages into ten members (in descending order, Chang 1 to Chang 10) (Fig. 2). The Chang 7 member is

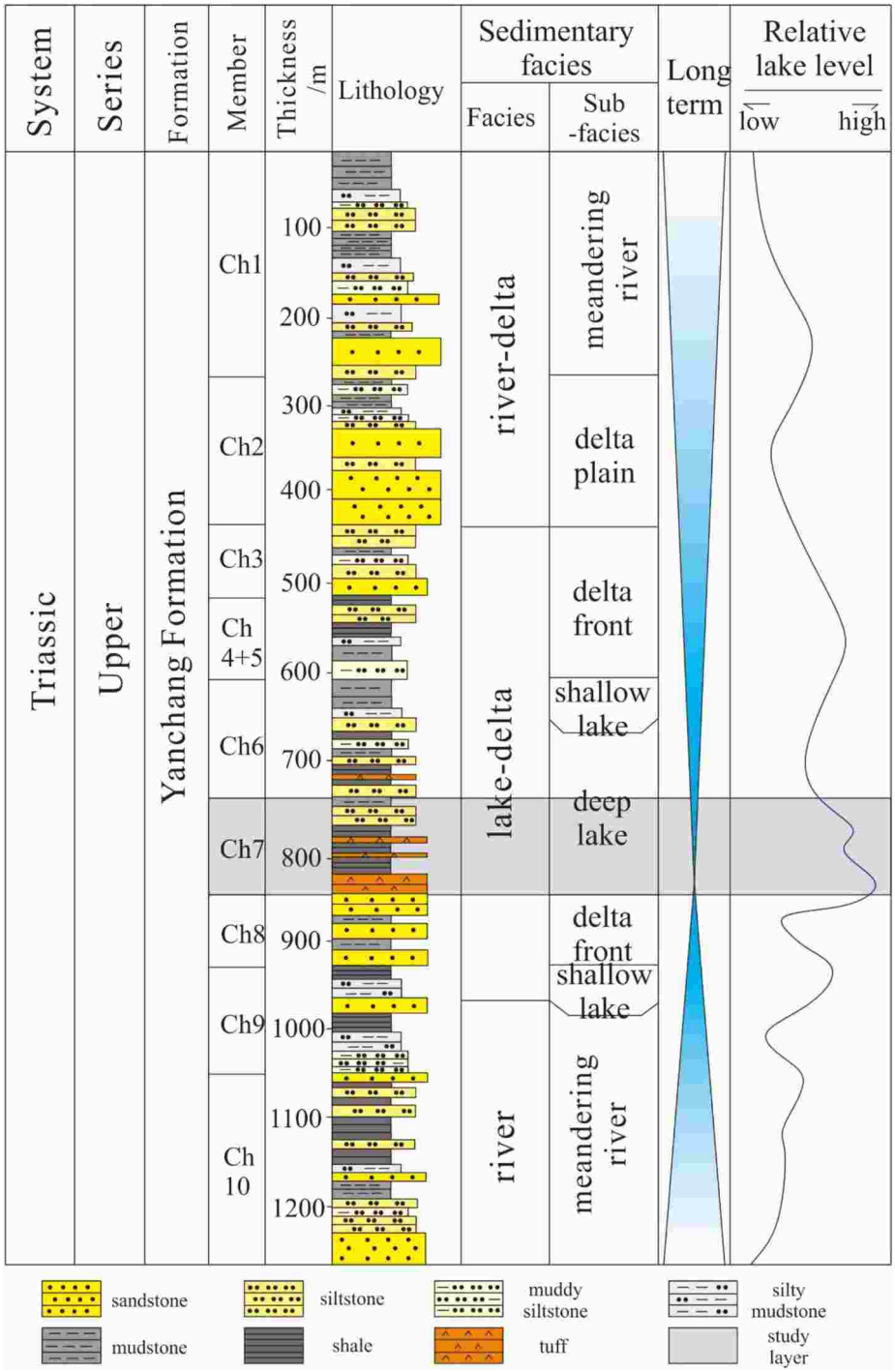

Fig. 2. Stratigraphy, thickness, lithology, sedimentary facies, and relative lake level of the Upper Triassic Yanchang Formation in the Ordos Basin (modified from Qiu et al., 2015a; Liu et al., 2016).

further subdivided into three parts from bottom to top: Chang 7_3, Chang 7_2, and Chang 7_1 (Li et al., 2018). During deposition of the Chang 7 member, the lacustrine basin subsided and expanded significantly because of intense tectonic movements. Large-scale organic-rich shales and tuffs were deposited under semi-deep to deep-lake conditions. These organic-rich shales have been demonstrated to be the dominant high-quality hydrocarbon source rock for the Mesozoic oil pools in the Ordos basin (Qiu et al., 2015a,b). Tuff layers are widely developed in the Chang 7 member. The thicknesses of a single tuff layer ranges from several millimeters to tens of centimeters, and the cumulative thickness can reach several meters. Tuffs are most developed in the Chang 7_3 section, which mainly consists of a thick layer of black organic-rich shale that is interbedded with tuff layers (Fig. 2). The Chang 7 member of the Ordos Basin has become an attractive petroleum exploration target for unconventional oil and gas development (Tang et al., 2015; Dou et al., 2018).

3. Samples and methods

The samples used in this study were collected from cores and field outcrops. The tuff core samples were mainly from two exploration wells (Bin 1 and JH 4) in the Jinghe oilfield, which is located in the southwestern part of the Ordos Basin. Some samples were collected from the Yishicun outcrop, located on the southern margin of the Yishan slope (Fig. 1). The samples were examined by microscopic observations, X-ray diffraction (XRD), high-resolution field emission scanning electron microscopy (FE-SEM), and porosity and permeability analyses.

The XRD was used to identify mineral types and obtain mineral content of the tuff samples. The XRD determinations used a D8 DISCOVER system with Cu-Ka radiation, with a voltage of 40 kV, and current of 25 mA. The samples were first ground to <40 μm using an agate mortar and were then oven-dried at 40 °C for 2 days. Each sample was scanned from 3° to 70° with a step size of 0.02°. Computer analysis of the diffractograms provided the identification and semiquantitative analysis of the relative abundances (in weight percent) of the various mineral phases. Thin section point count was also used to analyze composition of the tuff rock by counting 300 points per thin section.

Optical microscopy of prepared thin sections and field emission-scanning electron microscopy (FE-SEM) were used to identify the texture and pore characteristics. The FE-SEM determinations were conducted using a FEI Quanta200F system. Ar-ion-beam milling was used to prepare the samples. The porosity and permeability data were obtained from the analyses of 2.5-cm plugs that were drilled from the cores. The porosity data were obtained from helium porosity measurements by using a Boyle's law porosimeter by Ultrapore-200A. The permeabilities were measured by ULTRA-PERM™ 200.

4. Results

4.1. Core characteristics

A large number of tuffaceous layers are developed in Chang 7 member of the Ordos Basin. The tuff layers are commonly interbedded with shale (Fig. 3A–C), and sometimes the tuffaceous materials are mixed with clastic sediments. The thicknesses and frequencies of the tuff layers vary greatly vertically. The thicknesses of single tuff layers commonly range from a few millimeters to tens of centimeters, up to approximately 1 m at the bottom of the Chang 7_3 interval. The number of tuff layers are as great as 111 layers per meter. The net thickness of the tuff is as high as 38%.The tuffs in the Chang 7_3 cores are commonly oil-bearing (Fig. 3D–F). The tuff reservoir cores are commonly oil-stained. The fractures and pores in the tuff reservoirs were observed to be filled with oil. The oil shows observed in the cores suggest that the tuff reservoirs may hold large tight oil exploration potential.

4.2. Mineralogy and lithology

XRD analyses show that the mineral composition of the tuffaceous rocks in the study area mainly include quartz, feldspar, clay minerals, carbonate minerals, zeolite, and pyrite (Fig. 4). Quartz is the main mineral in the tuffaceous rocks ranging from 2.7 to 64.6 wt%, with an average of 41.5 wt%. Feldspar ranges from 11.1 to 63.3 wt%, with an average of 26.3 wt%. The total clay mineral content ranges between 2 and 50.2 wt%, with an average of 19.7 wt%. Carbonate minerals (mainly calcite), zeolite, and pyrite occur in some of the analyzed samples, with averages of 5.6 wt%, 11.7 wt%, and 6.4 wt%, respectively.

Based on the study obervations, the Chang 7_3 tuffaceous rocks in the study area are further divided into five lithology types: vitric tuff, crystal-vitric tuff, crystal tuff, tuffite, and tuffaceous sandstone. The mineral composition and content of the different lithologies vary greatly (Figs. 4 and 5).

4.2.1. Vitric tuff (VT)

Vitric tuff has a high vitric composition content (>75%). The vitric

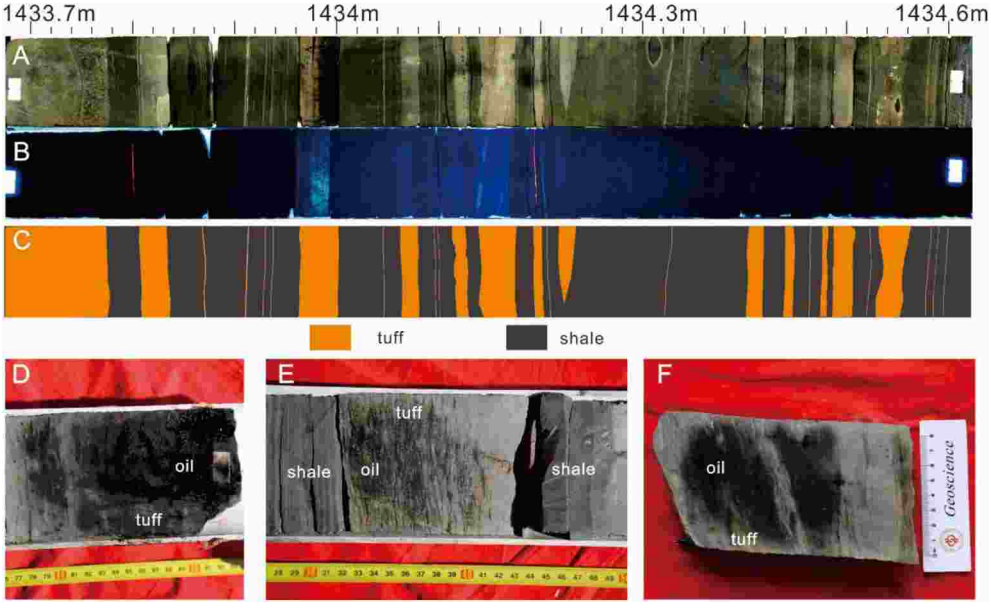

Fig. 3. Cores characteristics of the Chang 7 tuff. (A) Core photograph of tuff-layer-rich shale strata. Well Bin 1, 1433.7 m–1434.6 m. (B) Ultraviolet fluorescence photograph of tuff-layer-rich shale strata showing the luminescence of oil in the tuff-rich layers. Well Bin 1, 1433.7 m–1434.6 m. (C) Schematic diagram of tuff-layer-rich shale strata. Well Bin 1, 1433.7 m–1434.6 m. (D) Oil-stained core of the tuff reservoir, Well Bin 1, 1446.37 m. (E) Oil-stained core of the tuff reservoir, Well Bin 1, 1445.8 m. (F) Oil-stained core of the tuff reservoir, Well Bin 1, 1445.0 m.

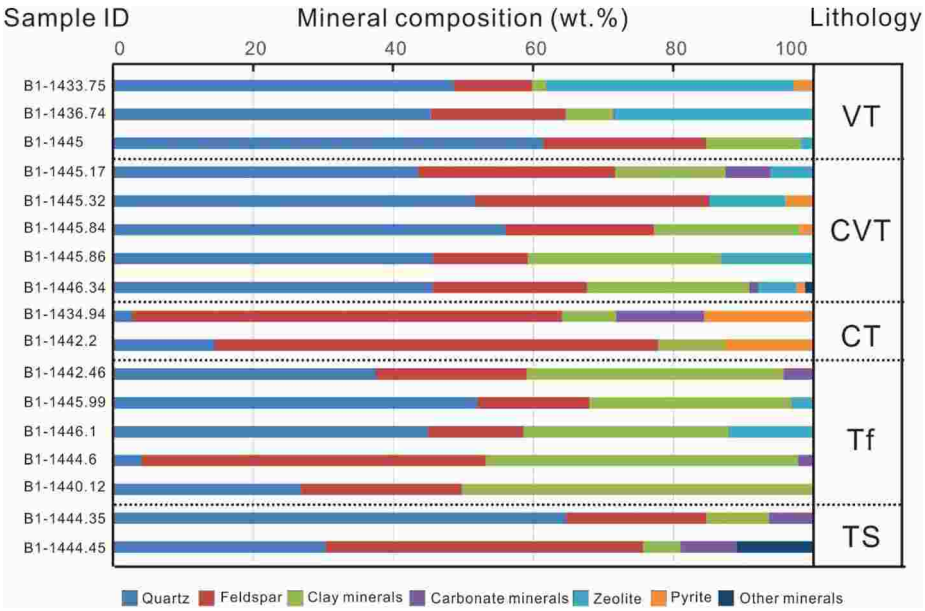

Fig. 4. Mineral composition of the tuff in the Chang 7 member. VT: Vitric tuff; CVT: Crystal-vitric tuff; CT: Crystal tuff; Tf: Tuffite; TS: Tuffaceous sandstone.

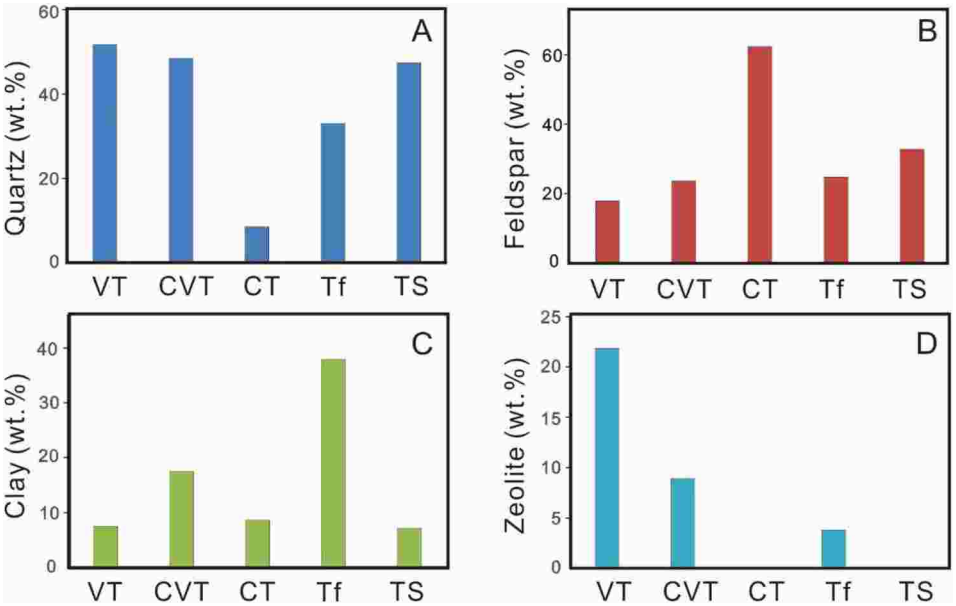

Fig. 5. Content of quartz, feldspar, clay, and zeolite in different lithologies. (A) Content of quartz in different lithologies. (B) Content of feldspar in different lithologies. (C) Content of clay in different lithologies. (D) Content of zeolite in different lithologies. VT: Vitric tuff; CVT: Crystal-vitric tuff; CT: Crystal tuff; Tf: Tuffite; TS: Tuffaceous sandstone.

tuff layers in the outcrop have gray-white or gray-yellow color. The thicknesses of single vitric tuff layers range from 2 cm to 20 cm. The horizontal distributions of the vitric tuff layers are continuous and the thicknesses are consistent over tens of meters in the outcrop.

The vitric fragments in the vitric tuff include rigid vitric fragments with various shapes (such as arc-shaped, crescent shaped, chicken bone shaped, irregular sharp angle shaped, and sponge bone needle shaped) and plastic irregular volcanic glass (Fig. 6 A and B). The rigid vitric fragments have clear boundaries and are easy to identify under plane-polarized light. The vitric fragments exhibit extinction under cross-polarized light. The sorting and rounding of the vitric fragments is poor. The diameters of the rigid vitric fragments range from <0.005 mm to 0.25 mm. The vitrinite tuffs are commonly altered.

The average XRD contents of quartz, feldspar, clay minerals, and zeolite in the vitric tuffs are 51.8 wt%, 17.87 wt%, 7.47 wt%, and 21.83 wt%, respectively. The quartz and zeolite contents in the vitric tuffs are higher than those for the other lithologies (Figs. 4 and 5).

4.2.2. *Crystal-vitric tuff (CVT)*

The crystal-vitric tuffs are mainly composed of vitric fragments (>50%) with crystal fragments between 25% and 50%. The crystal-vitric tuffs are mainly located at the bottom of the Chang 7_3 member. The thicknesses of single crystal-vitric tuff layers are consistent and range from 10 cm to 30 cm.

The light microscopy examinations showed that the sizes of the crystal fragments are commonly less than 1 mm, mostly between 0.1 and 0.5 mm, with irregular sharp, polygonal shapes or semicircular shapes. The sorting and rounding of the crystal fragments are poor. Most of the

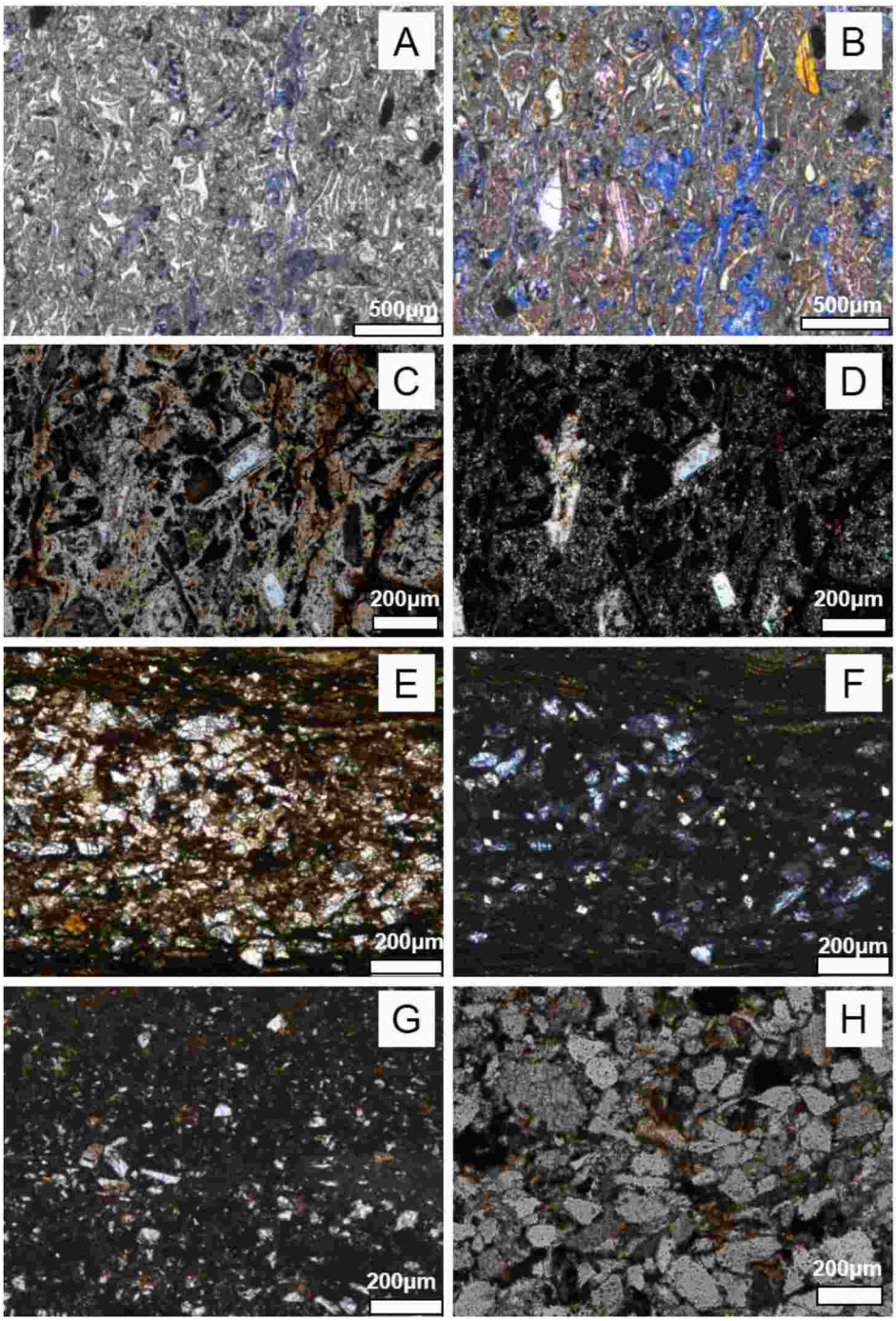

Fig. 6. Microphotographs of different tuff lithologies. (A) Vitric tuff, plane polarized light, from Yishicun field outcrop. (B) Vitric tuff, plane polarized light, cast thin-section from Yishicun field outcrop. (C) Crystal-vitric tuff, plane polarized light, Well Bin 1, 1446.34 m. (D) Crystal-vitric tuff, cross-polarized light, Well Bin 1, 1446.34 m. (E) Crystal tuff, plane polarized light, Well Bin 1, 1434.94 m. (F) Crystal tuff, cross-polarized light, Well Bin 1, 1434.94 m. (G) Tuffite, plane polarized light, Well Bin 1, 1441.17 m. (H) Tuffaceous sandstone, plane polarized light, Well Bin 1, 1444.25 m.

crystal fragments are composed of quartz and feldspar. Irregular cracks were observed within the surfaces of the quartz crystal fragments. The feldspar crystal fragments exhibit obvious cracks along cleavages, and portions of the feldspar crystal fragments have been dissolved or replaced. The vitric fragments have various shapes with different particle sizes, such as sponge needle shapes, arc shapes, arch shapes, and almond shapes (Fig. 6 C and D).

The composition of the crystal-vitric tuffs determined by XRD show quartz, feldspar and clay mineral averages of 48.5 wt%, 23.68 wt%, and 17.44 wt%, respectively. The average quartz content is slightly lower than that of the vitric tuffs. The average zeolite content decreased to 8.96 wt% compared to that of vitric tuff (Figs. 4 and 5).

4.2.3. Crystal tuff (CT)

The crystal tuffs are mainly composed of crystal fragments (>75%). These crystal tuffs mainly occur as intercalations in the "Zhangjiatan" shale (organic-rich shale in the Chang 7_3 member) in the form of laminae or thin layers. The crystal fragments in the crystal tuffs consist mainly of feldspar or quartz. The sizes of the crystal fragments range from silty-grade to fine-grade, with a maximum size of 0.25 mm. The sorting of the crystal tuffs is better than those of the vitric and crystal-vitric tuffs. The crystal fragments commonly have irregular cracks and harbor edge shapes (Fig. 6 E and F). Some of the plagioclase crystal fragments are euhedral with fractures along the cleavages.

Feldspar is the predominant mineral present in the crystal tuffs, with an average of 62.4 wt%. The average quartz and clay minerals contents are 8.6 wt% and 8.55 wt%, respectively. Zeolites are not observed in the

crystal tuff samples (Figs. 4 and 5).

4.2.4. Tuffite (Tf)

The tuffites are a transitional rock type that is intermediate between pyroclastic rock and sedimentary rock, with pyroclastic material contents between 50% and 90% and grain sizes less than 2 mm. The color of tuffite is gray black or gray-yellow. The tuffite particle sizes commonly range from silty-grade to fine-grade. The thicknesses of single tuffite layers are relatively thick and range from 10 cm to 30 cm.

Terrigenous clastic materials are also present in addition to crystal fragments, vitric fragments, and volcanic glass (Fig. 6G). The terrigenous clastic components consist mainly of quartz, feldspar, and clay matrix materials. The terrigenous clastic quartz and feldspar grains are commonly rounded and smooth without obvious cracks. Some of the grain edges have been eroded, and altered into clay minerals.

The XRD results show that the average content of the quartz,

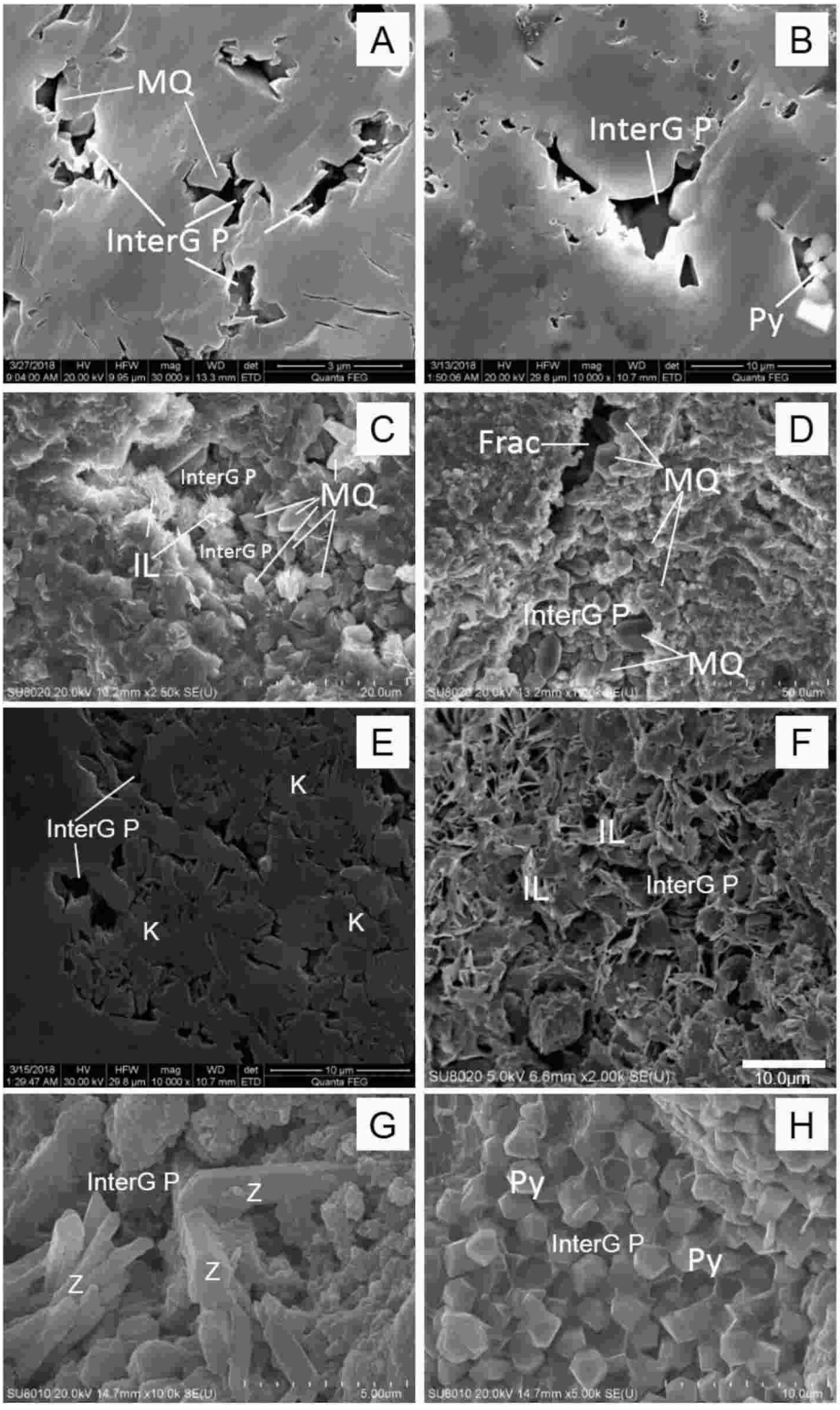

Fig. 7. Microphotographs of intergranular pores in the tuff reservoir. (A) Intergranular pores between microquartz, Well Bin 1, 1446.1 m. (B) Intergranular pores between microquartz and pyrite, Well Bin 1, 1446.34 m. (C) Intergranular pores between microquartz and illite. Large amounts of microcrystalline quartz formed by devitrification can be observed. Well Bin 1, 1445.1 m. (D) Fracture and intergranular pores between microquartz, with large amounts of microcrystalline quartz formed by devitrification; Well Bin 1, 1445.1 m. (E) Intergranular pores between kaolinite, Well Bin 1, 1446.34 m. (F) Intergranular pores between illite, Well Bin 1, 1446.34 m. (G) Intergranular pores between zeolite, Well Bin 1, 1445.75 m. (H) Intergranular pores between pyrite, Well Bin 1, 1445.75 m. InterG P: Intergranular pore; MQ: microquartz; IL: illite; Frac: fracture; K: kaolinite; and Z: zeolite.

feldspar, clay, and zeolite in the tuffite are 33.04 wt%, 24.68 wt%, 37.9 wt%, and 3.85 wt%, respectively (Figs. 4 and 5). The clay content of tuffite are higher than those of the other lithologies.

4.2.5. Tuffaceous sandstone (TS)

The tuffaceous sandstones are characterized by high content (>50%) of terrigenous clastic materials, which mainly consist of sandy grains, with small amounts of pyroclastic materials (<50%). The thicknesses of single tuffaceous sandstone layers range from 10 cm to 20 cm.

The color of the tuffaceous sandstones is grayish black or grayish yellow. The components of the tuffaceous sandstones mainly include quartz, feldspar, clay minerals, and mica. Sand-sized grains are clearly observed. The particle sizes range from silt to fine sand (Fig. 6H).

The XRD results show that the average quartz, feldspar, and clay minerals content in the tuffaceous sandstones are 47.45 wt%, 32.75 wt %, and 7.1 wt%, respectively (Figs. 4 and 5). The tuffaceous sandstones also contain some carbonate minerals (average 7.25 wt%).

4.3. Pore types

The pores in the tuff reservoirs are of various types and have different sizes and are divided into six types: (1) intergranular pores, (2) intragranular pores/cracks, (3) dissolution pores, (4) seams around grains, (5) organic matter related pores, and (6) fractures.

4.3.1. Intergranular pores

The intergranular pores, pores between detrital or authigenic particles, were observed in the tuffs mainly between quartz and feldspar grains. The intergranular pores are commonly well connected and form effective pore networks. The SEM observations revealed that the shapes of the intergranular pores vary and mainly form polygonal and irregular shapes (Fig. 7). The sizes of the intergranular pores commonly range from 60 nm to 20 μm, which indicate mostly nano-to micron-scale pores (Fig. 10). The abundance of intergranular pores is highest among all of the pore types.

Intergranular pores are also developed between authigenic clay minerals, zeolites, and pyrites in the tuffs (Fig. 7E–H). The sizes of those

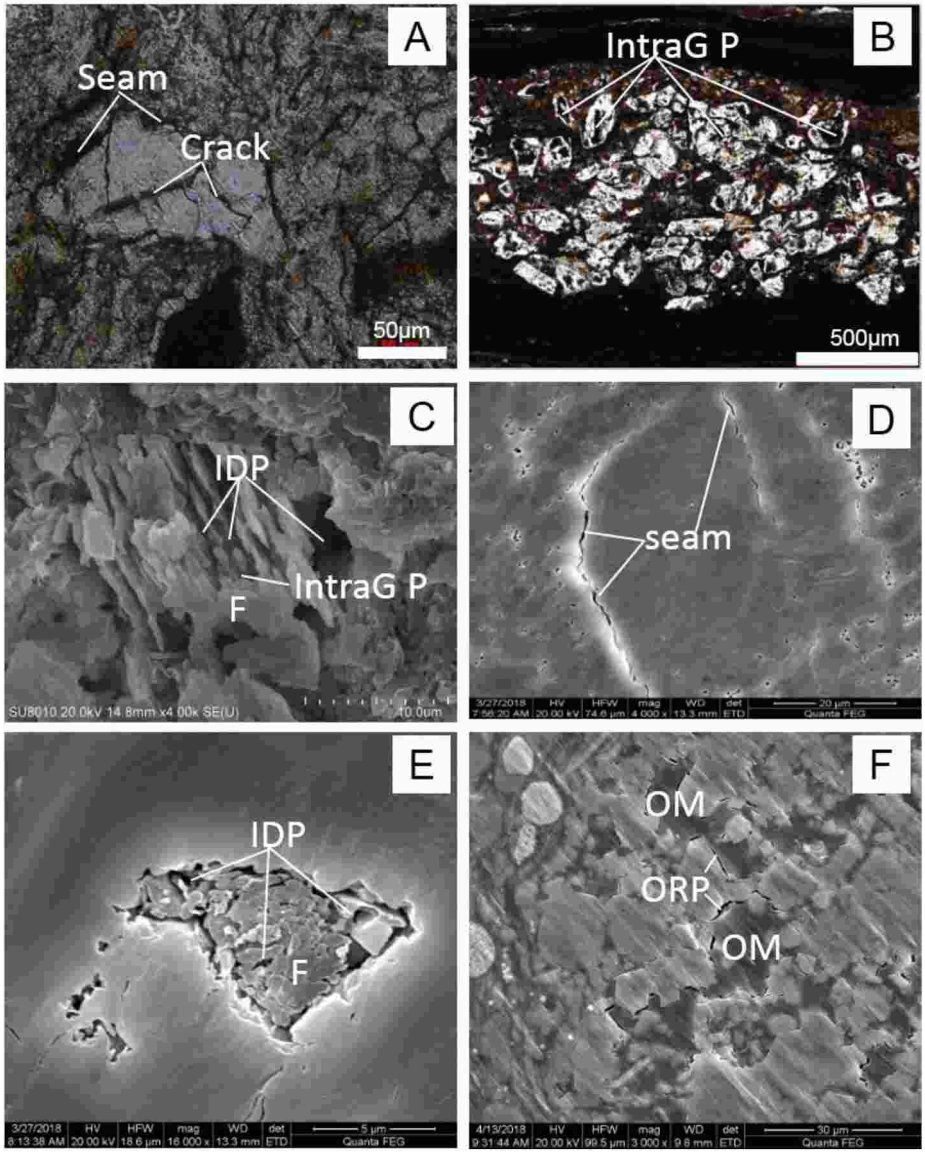

Fig. 8. Microphotos of various pore types in the tuff reservoir. (A) Seams around crystal fragments and cracks within crystal fragments. Well Bin 1, 1446.34 m. (B) Intragranular pores in crystal fragments. Well Bin 1, 1436.74 m (C) Intragranular dissolution pores in feldspar grains. Well Bin 1, 1445.93 m. (D) Seams around grains. Well Bin 1, 1446.1 m. (E) Intragranular dissolution pores in feldspar grain. Well Bin 1, 1446.1 m. (F) Organic matter related pores. Well Bin 1, 1445.96 m.

relatively small, most of which are microporous. The phyllosilicate pores commonly have slit-like shapes, with diameters ranging from tens of nanometers to several microns (Fig. 7 E, F). The intergranular pores are well developed between authigenic zeolite crystals, with diameters up to approximately 3 μm (Fig. 7 G). The intergranular pores between the pyrite crystals commonly have polygonal shapes, with diameters between 20 nm and 2 μm (Fig. 7 H).

4.3.2. Intragranular pores/cracks

The intragranular pores/cracks are developed within grains in the tuffs. According to their different characteristics and formation mechanisms, the intragranular pores/cracks can be further divided into three types.

(1) Cracks within crystal fragments

Cracks are often observed within crystal fragments in the tuffs. These cracks commonly develop along the cleavages or weak parts in crystal fragments and exhibit irregular shapes or interlaced network structures (Fig. 8A). The cracks within the crystal fragments in the tuff are often caused by the release of great amounts of energy when magma erupts, or by the sudden drops in pressure and temperature when the crystal fragments are ejected from the underground (Zhang et al., 2013).

(2) Intragranular dissolution pores

The feldspar content in the tuffs is relatively high. Since feldspar is easily dissolved, intragranular dissolution pores are mainly developed within feldspar grains. The shapes and sizes of the intragranular dissolution pores in the feldspar grains vary due to the differing degrees of dissolution. The intragranular dissolution pores in the feldspar grains can be arc-shaped, polygonal shaped, and irregularly shaped, with diameters from 10 nm to 700 nm (Fig. 8 C and E).

(3) Gas escape pores

Pyroclastic materials commonly contain volatile gases present during eruptions. Expulsion of volatile gases following eruptions create intragranular pores within vitric or lithic fragments (Guo et al., 2013). These pores commonly have oval-shapes or irregular shapes (Fig. 8B).

The sizes of the intragranular pores are relatively small, which commonly range from 10 nm to a few microns, and the abundance of the intragranular pores is relatively low (Fig. 10).

4.3.3. Seams around grains

Seams were observed surrounding crystal fragments, rigid vitric fragments, and debris grains (Fig. 8 A and D). These seams probably formed due to the large compositional differences between the grains and matrix. The seam shapes, which are limited by the shapes of the grains, are commonly long and narrow. The seams can act as the channels for fluid migration and reservoir storage space.

4.3.4. Dissolution pores

The shapes of the dissolution pores are irregular and exhibit arc- or crescent-shapes. There are obvious corrosion marks on the edges of the dissolution pores (Fig. 9). The diameters of the dissolution pores range from <1 μm up to approximately 2 mm (Figs. 9 and 10). The dissolution pores are mainly developed in the thick tuffs in the lower part of the Chang 7_3 member.

The dissolution pores are often accompanied by bedding and fractures (Fig. 9 A and B). The ultraviolet (UV) fluorescence photomicrographs show luminescent oil in the dissolution pores (Fig. 9B–D).

4.3.5. Organic matter related pores

The tuffs close to the shales with high-organic contents also contain certain amount of organic matter. The organic matter related pores in the tuffs are mainly shrinkage seams at the edges of the organic matter. The shrinkage seams at the edges of the organic matter are developed between the edges of the organic matter and the inorganic particles (Fig. 8F). The widths of the shrinkage seams at the edges of the organic matter in the tuffs are commonly less than 1 μm (Fig. 10). The organic matter in the tuffs is commonly nonporous except for a few seams at the mineral/grain contacts. Since organic matter pore is a functions of thermal maturity, lacking pores developed within organic matter in the tuffs is mainly due to low thermal maturity of the samples in the study area (typically <0.8% Ro vitrinite reflectance). The SEM images show that organic matter in the tuffs are commonly void-filling, indicating a secondary type of organic matter interpreted as solid bitumen (Camp, 2017, 2019; Valentine and Hackley, 2019). It is possible that this solid bitumen is residual oil that has migrated into the tuff from the underlying organic-rich shale (Camp, 2019; Wood et al., 2015). This type of organic matter commonly occludes the pre-existing intergranular pores (organic matter cement) and thus it is detrimental for reservoir quality (Wood et al., 2015). The organic matter content in the tuffs is limited, so the amount organic matter-related pores are relatively low (Fig. 10).

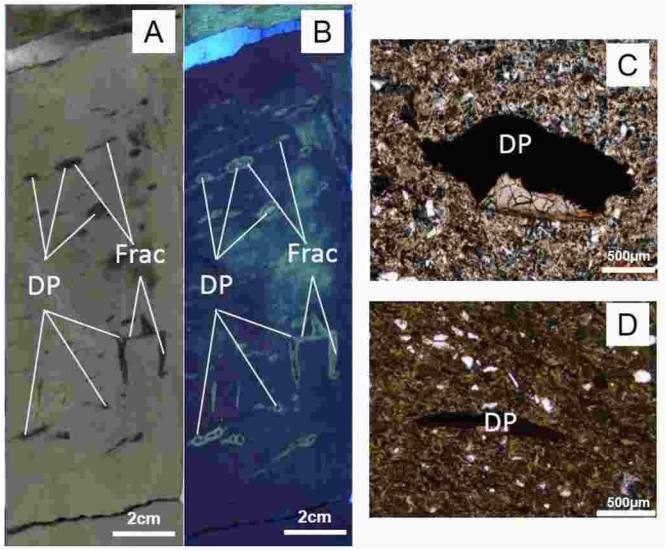

Fig. 9. Cores and microphotographs of dissolution pores in the tuff reservoir. (A) Core photograph of the tuff reservoir showing dissolution pores and fractures filled with oil. Well Bin 1, 1445.2 m. (B) Ultraviolet fluorescence photograph of the tuff reservoir showing dissolution pores and fractures filled with oil. Well Bin 1, 1445.2 m. (C) Microphotograpphs of dissolution pores in the tuff reservoir with residual oil. Well Bin 1, 1445.17 m. (D) Microphotographs of dissolution pores in the tuff reservoir. Well Bin 1, 1445.17 m. DP: dissolution pore; Frac: Fracture.

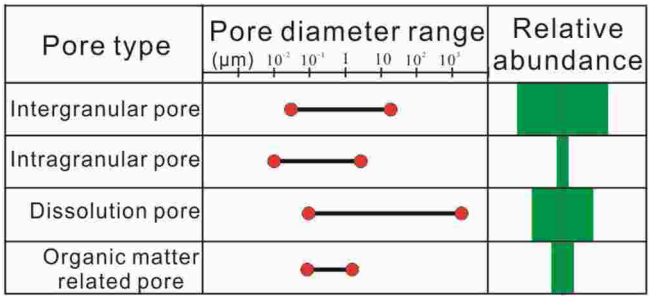

Fig. 10. Diameter ranges and relative abundance of different pore types in the tuff reservoir.

4.3.6. Fractures

A variety of fractures are present in the tuffs, including structural fractures (such as high-angle fractures and low-angle fractures) and diagenetic fractures (Fig. 9). High-angle shear fractures are the main structural fracture type in the tuff. In addition, there are many low-angle shear fractures. The extension heights of the structural fractures commonly range from 10 cm to 20 cm. In addition to the structural fractures, diagenetic fractures (mainly bedding fractures) are also developed in the tuffs. The diagenetic fractures are mostly developed along bedding planes, especially at the contact areas between the tuff lamina and organic-rich lamina.

4.4. Porosity and permeability

The porosities of the tuff reservoirs range from 2.33% to 12.62%, with an average of 7.2%. The permeability values are between 0.0005 mD and 0.281mD, with an average of 0.078mD. The porosities of the tuff reservoirs are generally positively correlated with the permeabilities (Figs. 11 and 12).

There are obvious porosity and permeability differences among the different lithologies. The vitric tuff porosities range from 8.46% to 12.61% (average 10.11%), and the permeabilities range from 0.111mD to 0.281mD (average 0.196 mD). The crystal-vitric tuff porosities range between 4.53% and 9.73% (average 6.25%) and the permeabilities are between 0.004 mD and 0.088 mD (average 0.063 mD). The crystal tuff porosities and permeabilities range between 5.05% and 6.33% (average 5.69%), 0.002 mD and 0.097 mD (average 0.049 mD), respectively. The porosities and permeabilities of the tuffites range between 2.33% and 6.12% (average 3.87%) and 0.0004 to 0.099 mD (average 0.102 mD), respectively. The porosities and permeabilities of the tuffaceous sandstones range from 6.45% to 8.24% (average 7.34%) and from 0.009 mD to 0.106 mD (average 0.057 mD), respectively (Fig. 11).

5. Discussion

5.1. Effectiveness of the tuff reservoir

Zou (2011) has shown that oil molecules can be stored in and pass through pores with diameters larger than 50 nm (Zou, 2011). Although the tuff reservoir has very low porosities and permeabilities, most diameters for the different pore types are larger than 50 nm (Fig. 10). Oil has been widely observed in the tuff as evidenced by staining (Fig. 3) and fluorescence (Fig. 9). The cores of tuff reservoirs are commonly oil-bearing. The oil stained and oil potted tuff cores account for approximately 40% of the whole tuff core of well Bin 1 at the lower part of the Chang 7_3 member. The average oil saturation of the tuff reservoir is approximately 40%. These results indicate that the tuff reservoir is effective for oil and gas accumulations.

Shales have been confirmed to be effective petroleum reservoirs and contain a variety of nanopores and micronpores (e.g., Loucks and Ruppel, 2007; Loucks et al., 2009, 2012; Slatt and O'Brien, 2011; Curtis et al., 2012). Commercial flow rates can be established from shale reservoirs after hydraulic fracture stimulation. The shales of the Chang 7_3 section in the study area have bulk porosities ranging from 1.60% to 6.33% (with an average of 3.06%) and permeabilities from 0.0001 mD to 0.016 mD (with an average of 0.0013 mD). The tuff porosities range from 2.33% to 12.61% (average 6.29%), and their permeabilities range from 0.0004 to 0.281 mD (average 0.064 mD) (Fig. 12). The average porosity and permeability of tuffs are clearly higher than those of the shales. Therefore, the tuff reservoirs can act as petroleum enrichment zones in the shale strata series. In 2019, well Chengye 1 in Ordos Basin got high oil product (121.38 t/d) in the Chang 7_3 member after fracturing. The reservoir porosities of well Chengye 1 are between 2% and 8%, with an average of 5% (Fu et al., 2020). The average porositis of tuffs are higher than that of Chengye 1 reservoir, suggesting that the tuff reservoir have good potential and can be effectiveness petroleum reservoirs after artificial fracturing.

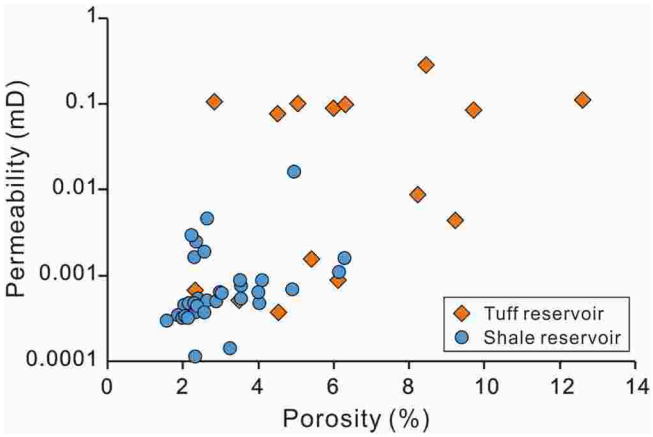

Fig. 12. Porosity versus permeability of the tuff reservoir and shale reservoir.

It is worth noting that there are many methods to measure porosity and permeability of shale and tight reservoirs, such as Gas Research Institute (GRI), nuclear magnetic resonance (NMR), mercury injection capillary pressure (MICP), and gas injection porosimetry (GIR) methods (Luffel and Guidry, 1992; Yao et al., 2010; Sigal, 2013; Sun et al., 2016). It is not surprising for results to vary from different methods. The porosity data in this study were obtained from helium porosity measurements by using a Boyle's law porosimeter, which is a frequently used and effective method of measuring porosity (Sun et al., 2016; Li et al., 2015; Yang et al., 2015). However, the porosity value obtained from this method are generally regarded to underestimate shale porosity, because the nano-sized pores and incomplete hydrocarbon cleaning prevents

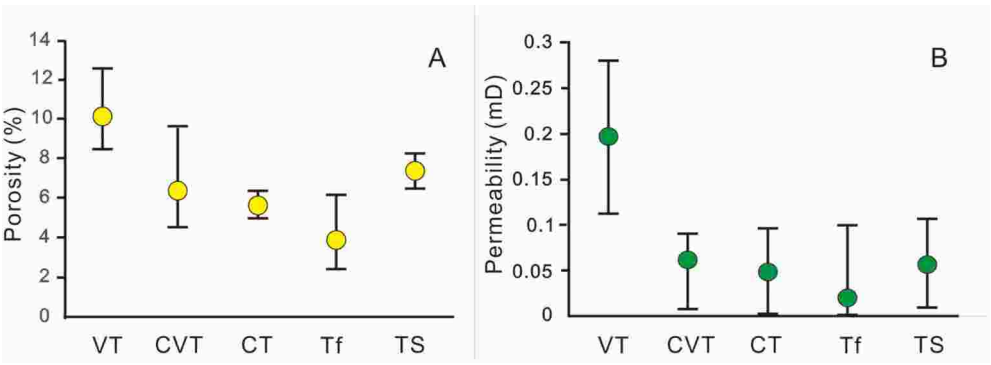

Fig. 11. Porosity and permeability characteristics of different lithologies. (A) Porosity characteristics of different lithologies. (B) Permeability characteristics of different lithologies.

helium from entering the pores and thus results in low measured porosity (Luffel and Guidry, 1992; Sun et al., 2016). Thus, the actual porosities of the tuff and shale reservoirs might be higher than the measured porosity present in this study.

The intergranular pores and dissolution pores have relatively higher abundances than the other observed pore types and are commonly well connected, forming an effective main pore network. The intragranular pores are commonly isolated and have relatively small and few pore throats. The contents of organic matter-related pores are also low due to the low organic matter contents in the tuffs. The intragranular and organic matter pores appear to lack sufficient connectivity to form effective pore networks.

5.2. Factors controlling reservoir quality

Although the reservoir qualities of the tuffs are generally better than those of shale, the tuff reservoir has strong heterogeneity (Figs. 11 and 12). The oil contents in the tuff reservoir also vary greatly (Fig. 13). The tuff reservoir quality can be a function of many controls, including depositional controls (such as lithology, grain size, component) and diagenetic controls (such as devitrification, alteration, and dissolution).

5.2.1. Lithology

The lithology is the basis of the original physical properties of reservoirs and later diagenetic transformations. Different lithologies have different compositions and texture characteristics, which result in different pore types and diagenesis processes (Macquaker and Davies, 2008; Wei et al., 2016; Li et al., 2020b). The tuff lithologies have a great influence on the tuff reservoir storage types and reservoir qualities. There are obvious differences in reservoir quality among the different tuff lithologies.

The porosities and permeabilities of the vitric tuffs are highest among all of the tuff lithologies, which are followed by crystal-vitric tuffs, tuffaceous sandstones, and crystal tuffs. The tuffites have relatively poor reservoir qualities, with low porosities and permeabilities (Fig. 11). The results show that the tuff lithologies have great impacts on the physical properties of the tuff reservoirs.

The vitric tuffs contain large amounts of rigid and plastic volcanic glass, which are prone to devitrification and dissolution and result in high reservoir quality (discussed below). There are plenty of intergranular pores and microfractures in the vitric tuffs, indicating good reservoir performance (Fig. 6B). Cracks within the crystal fragments and seams around grains are often present in the crystal fragments-rich tuff due to the influence of volcanism and compositional differences between the grains and matrix. However, crystal fragments are harder to devitrify than volcanic glass. Thus, the reservoir qualities of the crystal-vitric tuffs, tuffaceous sandstones, and crystal tuffs are inferior to those of the vitric tuffs. The tuffites have mixed composition of shale and pyroclastic material. Because shale has lower porosity and permeability than tuff, the tuffite has the lowest reservoir quality among all of the lithologies.

5.2.2. Grain size

The grain sizes in the tuff reservoirs vary vertically in single tuff layers. Based on the observation of the well drilling cores and field outcrops, the tuff layers at the bottom of Chang 7_3 section contain obvious normal grain size sequences. A sequence profile of well Bin 1 (interval 1445.9 m–1446.4 m) is shown in Fig. 14. In this sequence, the grains at the bottom of the sequence have the largest diameters (average 96.6 μm) and highest plane porosities 7.6% with good oil displays. The grains in the middle part of the sequence have a medium particle sizes (average 39.6 μm), and plane porosities of 6.1%. The grains in the upper part of the sequence have the smallest particle sizes (average 27.4 μm), and the plane porosities are 4.1%, which are also the lowest in the sequence. That is, from bottom to top in the sequence the grain sizes become finer, and the pore sizes and porosities decrease accordingly.

Tuffs with large grains size (e.g., crystal fragments and rigid vitric fragments) commonly have high primary porosities and large primary pores, which include primary intergranular pores, seams around grains, and cracks within vitric fragments. High primary porosities and large primary pores can be conducive to the entry of late diagenetic fluids (such as the organic acidic fluids formed by the thermal evolution of organic matter in the adjacent shales), which cause the tuff reservoir to be more prone to devitrification and dissolution with a further improvement in the reservoir quality. In contrast, tuffs with small grain sizes commonly have low primary porosities and small primary pores and are not easily modified by late diagenetic fluids. Therefore, grain size is an important factor that affect the physical properties of the tuff

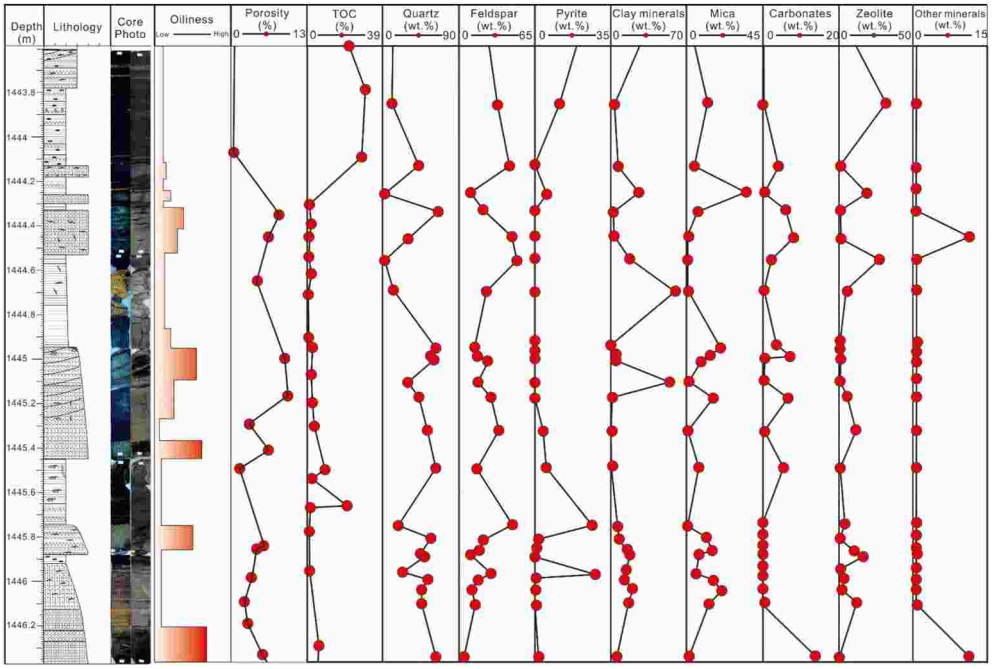

Fig. 13. Lithology, oiliness, porosity, TOC, and mineral composition characteristics of Well Bin1.

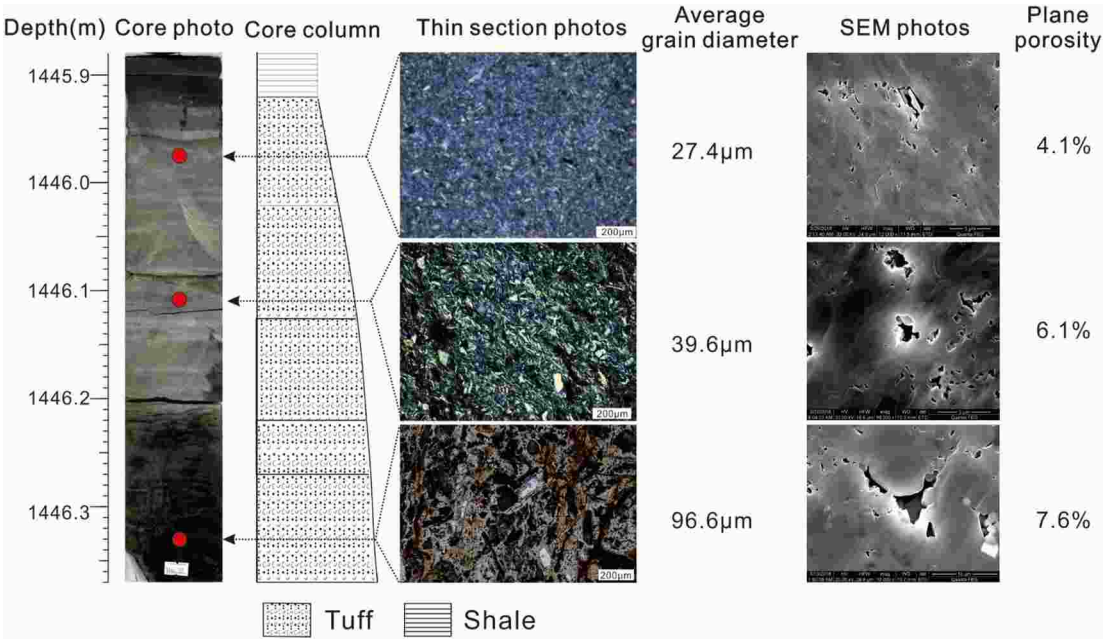

Fig. 14. Variation characteristics of particle sizes and porosities of a normal sequence in the core of well Bin 1 (interval 1445.9 m–1446.4 m).

reservoirs. Tuffs with large grain sizes commonly have good reservoir quality while tuffs with small grain sizes have poor reservoir quality (Fig. 14).

5.2.3. Component

The components of the different lithologies vary greatly (Figs. 4 and 5). The relative abundances of different minerals have various effects on the reservoir properties. Quartz is the predominant mineral in the tuffs. The quartz content in the vitric tuffs and crystal-vitric tuffs are high while the quartz contents in crystal tuffs and tuffites are low (Fig. 5A). The quartz present in the vitric tuffs and crystal-vitric tuffs is characterized by euhedral crystals, authigenicity, and microcrystalline structures (Fig. 7 C and D). Microcrystalline euhedral quartz might be formed by the devitrification of volcanic glass, which can transform volcanic glass to microcrystalline quartz and produce large numbers of intergranular pores between the microcrystalline quartz crystals (discussed

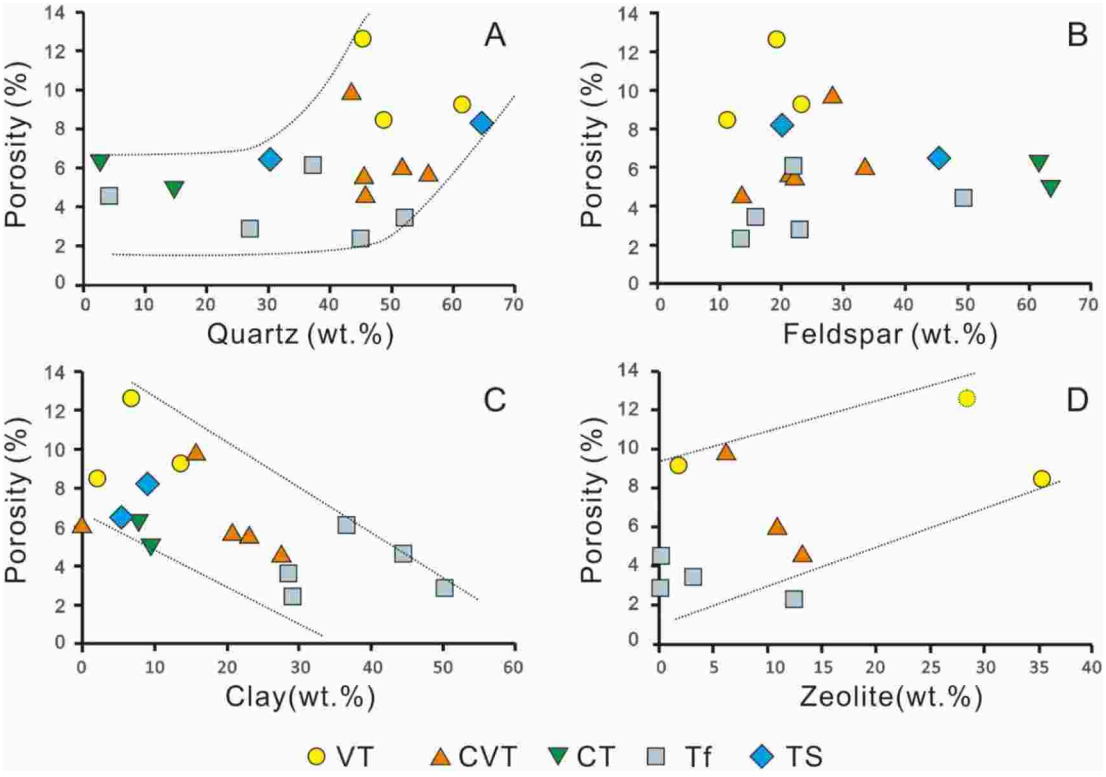

Fig. 15. Bulk porosities versus different mineral contents. (A) Bulk porosity versus quartz content. (B) Bulk porosity versus feldspar content. (C) Bulk porosity displays a negative covariation with clay content. (D) Bulk porosity displays a positive covariation with zeolite content.

below). A high microcrystalline quartz content indicates high intensity devitrification. The bulk porosities have a positive covariation with quartz contents when the quartz contents are greater than 40 wt% (mainly vitric tuffs and crystal-vitric tuffites) (Fig. 15A). In contrast, the quartz in the crystal tuff consists mainly of crystal fragments that were formed by volcanic eruptions while the quartz in the tuffites and tuffaceous sandstones consists mostly of detrital quartz. There is no obvious correlation between the porosity and quartz content when the quartz contents are below 40 wt% (mainly crystal tuffs and tuffites) (Fig. 15A).

Feldspar is another important mineral in the tuff reservoirs. There is no obvious relationship between the porosity and feldspar content (Fig. 15B). Feldspar is unstable under acidic conditions and is easily dissolved and converted to clay minerals (Rossel, 1982; Bjolykke, 1998). There is no doubt that feldspar dissolution can form secondary porosity and thus improve reservoir quality. The low feldspar contents of the initial compositions, such as for tuffite, are not conducive to forming secondary dissolution pores and thus result in low porosities (Fig. 15B). However, the vitric tuffs have low feldspar contents but high porosities. The low feldspar contents in the vitric tuffs are possibly due to the dissolution of large quantities of feldspars in the lithology, because high levels of dissolution occurred in the vitric tuffs (Fig. 9), and many feldspars were observed that had dissolved and produced secondary dissolution pores (Fig. 8 C and E).

Certain clay mineral contents were observed in the tuff reservoirs (Figs. 4 and 5), including kaolinite, illite, illite-smectite mixed layer, chlorite, and smectite. Authigenic kaolinite commonly has well-crystallized and pseudohexagonal platelet shapes and forms vermicular or booklet textures. Kaolinite can occur both as a pore-filling cement and as a replacement product of feldspars (Fig. 7E). Illite and illite-smectite mixed layers are often observed in the samples with hair-like or sheet like shapes and commonly form in the pore spaces (Fig. 7C and F). During diagenetic processes, pore-filling authigenic clay minerals were produced by the alteration of volcanic glass and feldspar. The clay content shows a negative correlation with porosity, indicating that although clay minerals can develop microintergranular pores (Fig. 7E and F), they tend to occupy more pore space and thus decrease the porosity.

The zeolites in the tuffs are commonly finely crystalline and occur as microscopic or submicroscopic crystals with needle shapes (Fig. 7G). Although zeolites can originate from a variety of precursor materials, such as volcanic and impact glasses, aluminosilicate gels, and aluminosilicate minerals, volcanic glass is the major precursor material of zeolites (Hay and Sheppard, 2001). Zeolite forms more readily from glass than from crystalline materials (Hay and Sheppard, 2001). The alteration of volcanic glass during the burial diagenetic stage (20 °C–120 °C) can provide a material source for precursor zeolites, which is a common formation mechanism for authigenic zeolites (English, 2001; Zhu et al., 2019). Zeolites usually form in alkaline environments with high activity ratios of $(Na^{+}+K^{+}+Ca^{2+})/H^{+}$ and relatively high pH levels (principally 7–10) (Hay and Sheppard, 2001). Volcanic glass can react to form zeolites by a dissolution-precipitation process, which is commonly complex and has multiple stages. The glass is first transformed to clinoptilolite and/or mordenite at approximately 41–55 °C and then reacts to form analcime at temperatures of 84–91 °C and is followed by albite formation at 120–124 °C (Iijima, 1988, and references therein). High zeolite contents commonly represent high degrees of devitrification and alteration of volcanic glass. Thus, the bulk porosities exhibit a positive covariation with the zeolite contents (Fig. 15D).

5.2.4. Devitrification

Vitric glass is one of the main components of the tuffs in the study area, which are very unstable due to their thermodynamic properties and can be easily transformed into crystals, that is, devitrification (Marshall, 1961; McPhie et al., 1993). The devitrification process consists a series of geochemical processes, such as the recrystallization of glasses, dissolution-precipitation, migration and transformation of metal ions. The devitrification of volcanic glass can produce microcrystalline quartz and feldspars. Because volcanic glass is significantly less dense than the minerals formed by devitrification, when the glass undergoes crystallization, the crystals that form during devitrification occupy a smaller volume than the original glass, and micropores would be formed during this series of processes, that is, devitrification pores (Zhao et al., 2009; Zheng et al., 2018a). The transformation of volcanic glass to crystals commonly generates considerable porosity due to isovolumetric contraction (Mchenry, 2009; Kirov et al., 2011; Ma et al., 2015; Zheng et al., 2018b). Although devitrification pores are commonly small (micron scale), they can serve as important reservoir spaces because they have high degree of connectivity and high abundances (Zhao et al., 2009; Zheng et al., 2018b).

Under optical microscopes, fine crystalline materials have been observed, which are produced by devitrification, and exhibit a felsic texture (Fig. 6D). The microcrystalline euhedral quartz crystals that are produced by devitrification can be observed under SEM (Fig. 7C and D). The intergranular pores are developed between the microquartz particles, which can act as effective storage spaces for oil and gas.

Devitrification is influenced by many factors, such as the composition of volcanic glass, volcanic glass content, and type and intensity of fluid action. The devitrification of acidic glass commonly forms an increased number of microcrystals than that of basic glass, which result in better reservoir quality (Yang et al., 2020). High vitric composition contents are conducive to the occurrence of devitrification and the formation of large quantities of devitrification pores. Devitrification is significantly affected by fluid action. Organic acids can effectively promote the devitrification process (Yang et al., 2020). High organic acid contents and low pH conditions are favorable for devitrification.

The tuffs in the Chang 7_3 section in the study area were deposited under a deep to semi-deep lake environment and were interbedded with organic-rich shales. Large amounts of organic acidic fluids were produced during the thermal evolution of organic matter, which produced favorable conditions for devitrification. The tuffs in the study area have commonly been devitrified and formed large quantities of fine microcrystalline quartz and feldspars, which formed devitrification pores between the micro-authigenic crystals (Fig. 7). Devitrification pores are a very important pore type in the tuff reservoir.

Devitrification generally occurs in the vitric tuffs and crystal-vitric tuffs. Among all of the lithologies, the vitric tuffs have the highest volcanic glass contents and most intense devitrification, which cause the vitric tuffs to have the highest porosity and permeability among all of the lithologies (Fig. 11).

5.2.5. Dissolution

The devitrification of volcanic glass can form a variety of aluminosilicate minerals, such as orthoclase, anorthite, and zeolites. Aluminosilicate minerals are easily dissolved under the action of acidic fluids, which results in dissolution pores (Chipera and Bish, 2010). The devitrification pores that are formed by devitrification can be further dissolved to produce enlarged dissolution pores (Fig. 9). In addition to the materials formed by devitrification, organic acids can dissolve vitric fragments and unstable crystal fragments, to form secondary dissolution pores (McPhie et al., 1993; Chen et al., 2017).

The organic-rich shales in the Chang 7 member released large amounts of organic acids during the hydrocarbon generation process, which provided favorable conditions for dissolution. The pore spaces of the tuffs in the study area commonly underwent secondary dissolution, which significantly increased the porosities of the rocks. Large dissolution pores can occasionally be observed in cores that are filled by large quantities of crude oil, which indicates a relatively strong dissolution process (Fig. 9). Secondary dissolution is a key process for enhancing the porosity during the tuff reservoir diagenetic evolution.

5.2.6. Fluid pathway system

Devitrification and dissolution are both significantly affected by fluid action. Fluids, especially acidic fluids, can increase the intensities of devitrification, alteration, and dissolution (Zheng et al., 2018b) and result in good reservoir quality. The fluid pathway system controls the fluid activities and further affects the reservoir quality.

The scouring surfaces, bedding, fractures, and well-developed primary pores in the study area can act as permeable channels for the influx of diagenetic fluids. The devitrification and dissolution intensities are obviously influenced by the development of the fluid pathway system. The large dissolution pores are generally associated with fractures, bedding, or scouring surfaces, which can provide channels for fluid flow and contribute to the occurrence of dissolution (Fig. 9).

5.3. Formation and evolution model of pores

The reservoir quality of tuffs is controlled by many factors, such as lithology, grain size, components, devitrification, dissolution, and fluid pathway systems. After deposition, in the early stage of diagenesis, the tuffs were mainly composed of volcanic glass (vitric fragments) and crystal fragments. The pores types at this stage consisted of main cracks within crystal fragments and seams around the crystal fragments and rigid vitric fragments (Fig. 16A). The tuffs with large grain sizes commonly have relatively more cracks and seams at this stage.

During diagenesis, with the increased temperatures and pressures and the action of fluids, the thermodynamically unstable volcanic glasses in the tuffs underwent devitrification and transformed into crystals, such as microcrystalline quartz, feldspar, and zeolite. Considerable numbers of devitrification pores would be produced during the process of devitrification due to isovolumetric contraction (Fig. 16B). Devitrification was influenced by temperatures, holding times, compositions, and fluid interactions (Mchenry, 2009; Kirov et al., 2011; Zhao et al., 2009; Ma et al., 2015). Because the temperatures and holding times experienced by the tuffs in the study area were similar, the compositions and fluid interactions were the main factors that controlled the devitrification intensity. The tuffs with high contents of volcanic glass and fluid pathway systems commonly exhibit strong devitrification and thus high porosity.

Volcanic glass and feldspar are prone to be altered and produce authigenic clay minerals (Fig. 16C). Clay minerals can occur both as pore-filling cements and as replacement products of feldspars. Pore-filling clay minerals might occupy the pore spaces.

The pore spaces might further undergo secondary dissolution and produce enlarged dissolution pores (Fig. 16D). A number of soluble components, such as volcanic glass and feldspar, can be dissolved to form relatively large dissolution pores. Dissolution is also controlled by the tuff composition and fluid actions. Large amounts of volcanic glass provide material basis for dissolution. The tuffs with good fluid pathway systems are favorable for fluid movement and thus result in more intense dissolution. The devitrification of volcanic glass can produce abundant intergranular pores, which might be further enhanced through secondary dissolution, making devitrified tuff favorable reservoirs.

5.4. Different patterns of diagenetic and pore evolution

The tuffs display strong heterogeneity in their reservoir qualities and oil-bearing properties (Fig. 17). Different parts of the tuff reservoirs have different lithologies, components, textures, and fractures (Fig. 17A), which result in different diagenetic and pore evolution patterns (Fig. 17B–D).

In sequence I (interval 1445.92 m–1446.37 m of well Bin 1), a scouring surface developed at the bottom, and the lower part consisted of relatively course particles with relatively high primary porosities (Fig. 17A). The scouring surface and relatively high primary porosity sequence acted as a good fluid pathway system for diagenetic fluids and intensified the devitrification and dissolution, which resulted in good reservoir quality and high oil contents (Fig. 17B). In contrast, the tuffs in the upper part of sequence I with fine particles and poor fluid pathway systems have low degrees of devitrification and dissolution and thus poor reservoir quality (Fig. 17C).

The tuffs in the upper part of sequence II (interval 1444.95 m–1445.45 m of well Bin 1) also have small particles sizes, but it can be observed from the core and fluorescence observations that the lower part and upper part of sequence II both exhibit high oil contents. This is because the bedding and fractures were well developed in the upper part of sequence II (Fig. 17A), which promoted fluid activity and was conducive to devitrification and dissolution, resulting in relatively high porosities where fluid pathway systems developed (Fig. 17D).

6. Conclusions

Tuffs are often associated with organic-rich shales because water-laid tuffs can promote the primary productivity and enrichment of organic matter. Tuff reservoirs are widely developed in the Chang 7 member of the Ordos Basin, which are commonly oil-bearing. The tuffs are tight reservoirs with low porosity and permeability, ranging from 2.33% to 12.62% (average 7.2%) and 0.000518 mD to 0.281 mD (average 0.0783 mD), respectively. The average porosity and permeability of the tuff are obviously better than those of shales and the pores in the tuff reservoirs are often filled with oil residues, indicating that the tuff reservoirs are effective for oil and gas accumulation.

The tuff reservoir qualities have strong heterogeneity, which are significantly controlled by lithology, grain size, component, devitrification, dissolution, and fluid pathway systems. The tuffs in the study area are further divided into five lithologies: vitric tuff, crystal-vitric tuff, crystal tuff, tuffite, and tuffaceous sandstone. The compositions and grain size differences of the different lithologies result in different primary pore types and porosities, which further affect devitrification and dissolution. Vitric tuffs have the best reservoir qualities among all of the lithologies.

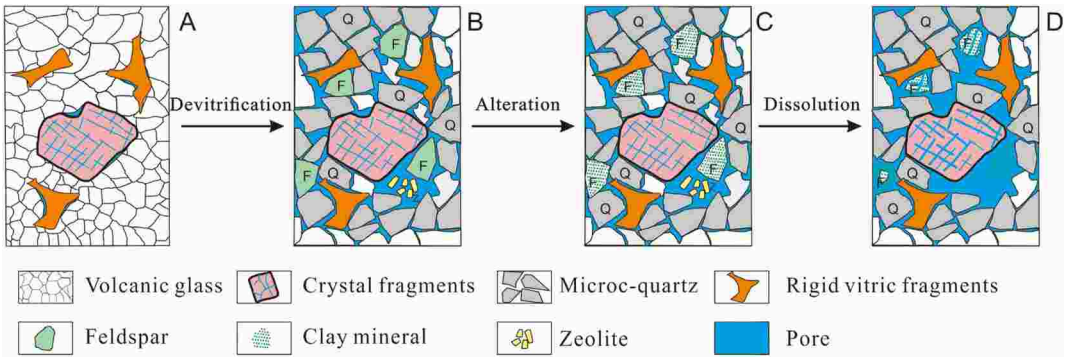

Fig. 16. Schematic model that shows the formation of pores in the tuff reservoir.

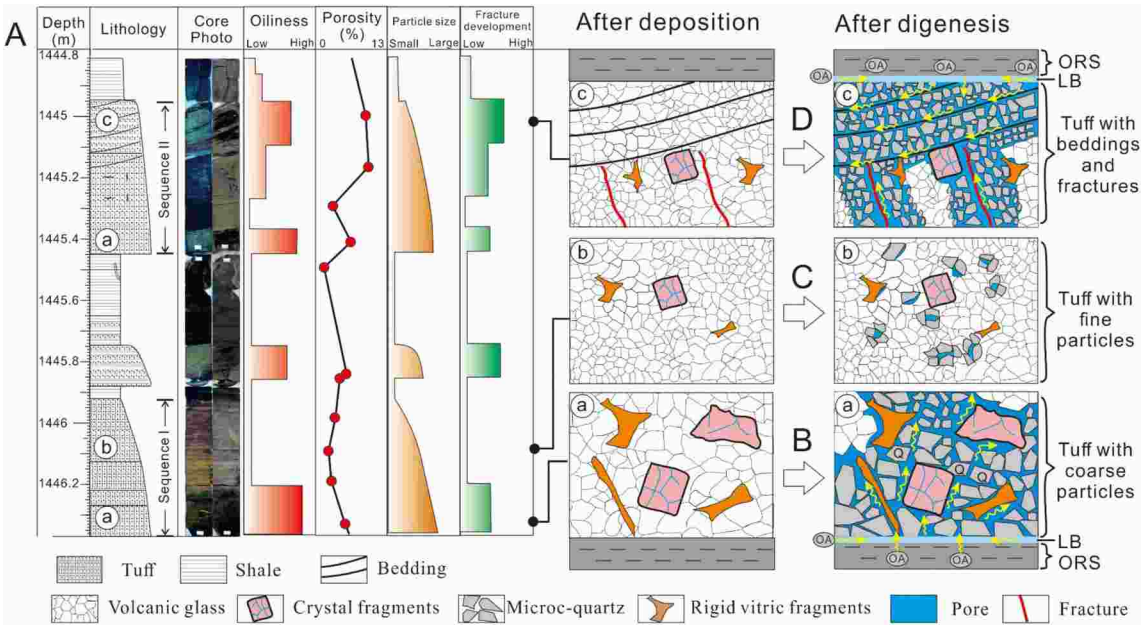

Fig. 17. Schematic model showing different diagenetic and pore evolution patterns in different parts of the tuff reservoir. (A) Lithology, oiliness, porosity, particle size, and fracture development characteristics of Well Bin1 (interval 1444.8 m- 1446.4 m). (B) Diagenetic and pore evolution tuff in the lower part of sequence I with coarse particles and scouring surface. (C) Diagenetic and pore evolution tuff in the upper part of sequence I with fine particles. (D) Diagenetic and pore evolution tuff in the upper part of sequence II with bedding and fractures. ORS: organic matter-rich shale; LB: layer boundary; OA: organic acid.

The secondary pores that were formed by devitrification and dissolution provide the main store spaces in the tuff reservoir. The devitrification of volcanic glass can produce abundant quantities of microcrystalline quartz, feldspars, and intergranular pores and can greatly improve the reservoir quality. The porosities exhibit a positive covariation with quartz contents in the vitric tuffs and crystal-vitric tuffs. The devitrification pores can be further dissolved to produce enlarged dissolution pores.

Both devitrification and dissolution are significantly affected by fluid action. The fluid pathway systems, including scouring surfaces, bedding, fractures, and well-developed primary pores, control the fluid activities and thus the intensities of devitrification and dissolution. Different parts of the tuff reservoirs have different lithologies, components, textures, and fractures, which result in different diagenetic and pore evolution patterns. Tuffs that contain high volcanic glass contents and coarse particles with abundant bedding and fractures are prone to intense devitrification and dissolution, resulting in high reservoir quality.

Tuffs have been demonstrated as favorable petroleum reservoirs in many oilfields worldwide (e.g., Gao et al., 2006; Zhang et al., 2010; Liu et al., 2014; Ma et al., 2016; Xu et al., 2017). However, the diagenesis and pore evolution process of fine-grained rocks are complex, especially tuff-rich fine-grained rocks. The control factors on tuff reservoir qualities in different area might be different due to various geological conditions. For example, different from the study area, the tuff reservoir quality of Tiaohu Formation in Santanghu Basin was mainly suggested to be controlled by organic matter content and burial depth (temperature) (Ma et al., 2015, 2016). Although the diagenesis and pore evolution process of tuff reservoir requires further research, this study provide useful insights to the process and controls of the diagenetic evolution of tuff reservoir in the Ordos Basin. Hopefully, this study will inspire further research on tuff-rich fine-grained rocks diagenesis that could positively impact future exploration and development strategies for tuff and shale hydrocarbon reservoirs.

Declaration of competing interest

The authors declare that they have no known competing financial interestsor personal relationships that could have appeared to influence the work reported in this paper.

Acknowledgments

We wish to acknowledge the constructive review by Wayne Camp and Luca Caracciolo for correcting errors and suggested revisions that helped to improve this article. This study was financially supported by the National Natural Science Foundation of China (Grant No. 41602137), the National Science and Technology Special (Grant No. 2017ZX05049- 006–001), the Strategic Cooperation Technology Projects of CNPC and CUPB (ZLZX 2020-02), and Science Foundation of China University of Petroleum, Beijing (No. 2462020YXZZ022).

References

Bjolykke, K., 1998. Clay mineral diagenesis in sedimentary basins — A key to the prediction of rock properties. Examples from North Sea Basin. Clay Miner. 33, 15–34.

Camp, W.K., 2017. Strategies for Identifying Organic Matter Types in SEM. American Association of Petroleum Geologists Search and Discovery Article 70233.

Camp, W.K., 2019. Diagenetic evolution of organic matter cements: implications for unconventional shale reservoir quality prediction. In: Camp, W., Milliken, K., Taylor, K., Fishman, N., Hackley, P., Macquaker, J. (Eds.), Mudstone Diagenesis: Research Perspectives for Shale Hydrocarbon Reservoirs, Seals, and Source Rocks. American Association of Petroleum Geologists Memoir 120, pp. 209–224.

Chen, Z., Wang, X., Wang, X., Zhang, Y., Yang, D., Tang, Y., 2017. Characteristics and petroleum origin of the Carboniferous volcanic rock reservoirs in the Shixi Bulge of Junggar Basin, western China. Mar. Petrol. Geol. 80, 517–537.

Chipera, S.J., Bish, D.L., 2010. Rehydration kinetics of a natural analcime. Eur. J. Mineral 22 (6), 787–795.

Curtis, M.E., Cardott, B.J., Sondergeld, C.H., Rai, C.S., 2012. Development of organic porosity in the Woodford Shale with increasing thermal maturity. Int. J. Coal Geol. 103, 26–31. https://doi.org/10.1016/j.coal.2012.08.004.

Desmastes, D., Grosheny, D., Beaudoin, B., et al., 2007. High resolution stratigraphic record constrained by volcanic ash beds at the Cenomanian—turonian boundary in the Western Interior. Basin,USA.Cretaceous Research 28 (4), 561–582.

Dong, H.L., Hall, C.M., Halliday, A.N., et al., 1997. $^{40}Ar/^{39}Ar$ illite dating of Late Caledonian (Acadian) metamorphism and cooling of K-bentonites and slates from the Welsh basin, UK. Earth Planet Sci. Lett. 150, 337–351.

Dou, W., Liu, L., Wu, K., et al., 2018. Diagenetic heterogeneity, pore throats characteristic and their effects on reservoir quality of the Upper Triassic tight sandstones of Yanchang Formation in Ordos Basin, China. Mar. Petrol. Geol. 98, 243–257.

English, P.M., 2001. Formation of analcime and moganite at Lake Lewis, central Australia: significance of groundwater evolution in diagenesis. Sediment. Geol. 143 (3), 219–244.
Fu, J.H., Li, S.X., Hou, Y.T., et al., 2020. Breakthrough of risk exploration of class II shale oil in chang 7 member of Yanchang Formation in the Ordos basin and its significance. China Petroleum Exploration 25, 78–92.
Gao, R.Q., Yang, J.B., Cong, P.D., et al., 2006. Analysis of the characteristics of tuffite reservoir in Erlian Oilfield. Well Logging Technol. 30 (4), 330—333 (in Chinese with English abstract).
Guo, X., Liu, L., Meng, Q., Yu, M., Yu, Z., Song, T., 2013. Reservoir characteristics and controlling factors of pyroclastic rocks of tongbomiao formation and nantun formation from tanan depression in tamtsag basin,Mongolia. Glob. Geol. 32 (2), 290–298 (in Chinese with English abstract).
Hay, R.L., Sheppard, R.A., 2021. Occurrence of zeolites in sedimentary rocks: an overview. Natural Zeolites Occurrence Properties & Applications 45 (1), 217–234.
He, C., Ji, L., Wu, Y., Su, A., Zhang, M., 2016. Characteristics of hydrothermal sedimentation process in the yanchang formation, south ordos basin, China: evidence from element geochemistry. Sediment. Geol. 345, 33–41.
Iijima, A., 1988. Diagenetic transformation of minerals as exemplified by zeolites and silica minerals— a Japanese view. Elsevier Science Publishers, Amsterdam. In: Chilingarian, G.V., Wolf, K.H. (Eds.), Diagenesis II, Developments in Sedimentology 43, pp. 147–211.
Kirov, G., Samajova, E., Nedialkov, R., Stanimirova, T.S., 2011. Alteration processes and products of acid pyroclastic rocks in Blgaria and Slovakia. Clay Miner. 46 (2), 279–294.
Lai, X.D., Yang, X.Y., Gao, P., Wu, B.L., Liu, C.Y., Sun, W.D., 2010. Geochemical study on U-rich tuffs in Yanchang Group in the southern Ordos Basin:Implications to their forming mechanism. Chinese Journal of Geology 45 (3), 757–776.
Li, L., Huang, B., Li, Y., et al., 2018. Multi-scale modeling of shale laminas and fracture networks in the Yanchang formation, Southern Ordos Basin. China. Eng. Geol. 243, 231–240.
Li, Q., Wu, S., Xia, D., You, X., Zhang, H., Lu, H., 2020a. Major and trace element geochemistry of the lacustrine organic-rich shales from the Upper Triassic Chang 7 Member in the southwestern Ordos Basin, China: implications for paleoenvironment and organic matter accumulation. Mar. Petrol. Geol. 111, 852–867.
Li, Q., You, X., Jiang, Z., Wu, S.m, Zhang, R., 2020b. Lithofacies and reservoir characterization of a source-controlled carbonate succession in a lacustrine rift basin, the Shulu Sag of Bohai Bay Basin, East China. J. Petrol. Sci. Eng. 192, 107180.
Li, X., Liu, P., Luo, Y., et al., 2015. Analysis of influencing factors on porosity measurement of shale gas reservoirs core. Prog. Geophys. 30, 2181–2187.
Liu, F., Zhu, X., Li, Y., Xue, M., Sun, J., 2016. Sedimentary facies analysis and depositional model of gravity-flow deposits of the Yanchang Formation, southwestern Ordos Basin, NW China. Aust. J. Earth Sci. 63 (7), 885–902.
Liu, Y.H., Zhu, X.M., Zhu, M., et al., 2014. Characteristics of tight oil reservoirs of the pennian fengcheng fomation in Wu—xia area, Junggar Basin. Lithologic Reservoirs 26 (4), 66–72 (in Chinese with English abstract).
Loucks, R.G., Ruppel, S.C., 2007. Mississippian barnett shale: lithofacies and depositional setting of a deep-water shale-gas succession in the fort worth basin, Texas. AAPG (Am. Assoc. Pet. Geol.) Bull. 91 (4), 579–601. https://doi.org/10.1306/11020606059.
Loucks, R.G., Reed, R.M., Ruppel, S.C., Jarvie, D.M., 2009. Morphology, genesis, and distribution of nanometerscale pores in siliceous mudstones of the Mississippian Barnett Shale. J. Sediment. Res. 79 (12), 848–861. https://doi.org/10.2110/jsr.2009.092.
Loucks, R.G., Reed, R.M., Ruppel, S.C., Hammes, U., 2012. Spectrum of pore types and networks in mudrocks and a descriptive classification for matrix-related mudrock pores. AAPG (Am. Assoc. Pet. Geol.) Bull. 96 (6), 1071–1098. https://doi.org/10.1306/08171111061.
Lowe, D.J., 2011. Tephrochronology and its application: a review. Quat. Geochronol. 6 (2), 107–153.
Luffel, D.L., Guidry, F.K., 1992. New core analysis methods for measuring reservoir rock properties of devonian shale. J. Petrol. Technol. 44 (11), 1184–1190.
Lyu, W., LianboZeng, Zonghu Liao, YuanyuanJi, PengLyu, Dong, Shaoqun, 2017. Fault damage zone characterization in tight-oil sandstones of the Upper Triassic Yanchang Formation in south Ordos Basin, China: integrating cores, conventional logs and image logs. Interpretation 5 (4), 27–39.
Ma, J., Huang, Z.L., Liu, Z.Z., Chang, C.C., Gao, X.Y., 2015. Tight reservoir characteristics of sedimentary organic matter-bearing tuff in Tiaohu Formation of Santanghu Basin. Earth Sci. Front. 22 (6), 185–196 (in Chinese with English abstract).
Ma, J., Huang, Z.L., Zhong, D.K., Liang, S.J., Liang, H., Xue, D.Q., Chen, X., Fan, T.G., 2016. Formation and distribution of tuffaceous tight reservoir in the permian Tiaohu formation in the malang sag, Santanghu Basin, NW China. Petrol. Explor. Dev. 43 (5), 714–722 (in Chinese with English abstract).
Macquaker, J., Davies, S., 2008. Lithofacies variability in fine-grained mixed clastic carbonate successions: implications for identifying shale-gas reservoirs. AAPG Annual Convention 20–23.
Marshall, R.R., 1961. Devitrification of natural glass. Bull. Geol. Soc. Am. 72, 1493–1520.
Mchenry, L.J., 2009. Element mobility during zeolitic and argillical teration of volcanic ash in a closed-basin lacustrine environment: case study Olduvai Gorge, Tanzania. Chem. Geol. 265, 540–552.
McPhie, J., Doyle, M., Allen, R., 1993. Volcanic Textures: a Guide to the Interpretation of Textures in Volcanic Rocks. University of Tasmania, Tasmania, pp. 17–28.
Qiu, X., Liu, C., Mao, G., Deng, Y., Wang, F., Wang, J., 2015a. Major, trace and platinum-group element geochemistry of the upper triassic nonmarine hot shales in the ordos basin, central China. Appl. Geochem. 53, 42–52.
Qiu, X.W., Liu, C.Y., Li, Y.H., Mao, G.Z., Wang, J.Q., 2009. Distribution characteristics and geological of tuff interlayers in Yanchang Formation of Ordos basin. Acta Sedimentol. Sin. 27 (6), 1138–1146 (in Chinese with English abstract).
Qiu, X.W., Liu, C.Y., Wang, F.F., Deng, Y., Mao, G.Z., 2015b. Trace and rare earth element geochemistry of the upper triassic mudstones in the southern ordos basin, central China. Geol. J. 50 (4), 399–413.
Rossel, N.C., 1982. Clay mineral diagenesis in roliegend aeolian sandstones of the southern north sea. Clay Miner. 17, 69–77.
Sigal, R.F., 2013. Mercury capillary pressure measurements on Barnett core. SPE Reservoir Eval. Eng. 16 (4), 432–442. https://doi.org/10.2118/167607-pa.
Slatt, R.M., O'Brien, N.R., 2011. Pore types in the Barnett and Woodford gas shales: contribution to understanding gas storage and migration pathways in fine-grained rocks. AAPG (Am. Assoc. Pet. Geol.) Bull. 95 (12), 2017–2030. https://doi.org/10.1306/03301110145.
Sun, J., Dong, X., Wang, J., 2016. Measurement of total porosity for gas shales by gas injection porosimetry (GIP) method. Fuel 186, 694–707.
Tang, X., Zhang, J., Jin, Z., Xiong, J., Lin, L., Yu, Y., et al., 2015. Experimental investigation of thermal maturation on shale reservoir properties from hydrous pyrolysis of chang 7 shale, Ordos basin. Mar. Petrol. Geol. 64, 165–172.
Valentine, B.J., Hackley, P.C., 2019. Applications of correlative light and electron microscopy (CLEM) to organic matter in the North American shale petroleum systems. In: Camp, W., Milliken, K., Taylor, K., Fishman, N., Hackley, P., Macquaker, J. (Eds.), Mudstone Diagenesis: Research Perspectives for Shale Hydrocarbon Reservoirs, Seals, and Source Rocks. American Association of Petroleum Geologists Memoir 120, pp. 1–17.
Wang, C., Wang, Q., Chen, G., He, L., Xu, Y., Chen, L., et al., 2017. Petrographic and geochemical characteristics of the lacustrine black shales from the upper Triassic yanchang formation of the Ordos basin, China: implications for the organic matter accumulation. Mar. Petrol. Geol. 86, 52–65.
Wang, J.Q., Liu, C.Y., Li, H., Wu, T.T., Wu, J.L., 2017. Geochronology, potential source and regional implications of tuff intervals in chang 7 member of Yanchang Formation, south of Ordos basin. Acta Sedimentol. Sin. 35 (4), 691–704 (in Chinese with English abstract).
Wei, W., Zhu, X.M., Meng, Y.L., et al., 2016. Porosity model and its application in fight gas sandstone reservoir in the southern part of West Depression, Liaohe Basin, China. J. Petrol. Sci. Eng. 141, 24–37.
Wood, J.M., Sanei, H., Curtis, M.E., Clarkson, C.R., 2015. Solid bitumen as a determinant of reservoir quality in an unconventional tight gas siltstone play. Int. J. Coal Geol. 150–151, 287–295. https://doi.org/10.1016/j.coal.2015.03.015.
Xian, B., Wang, J., Gong, C., Yin, Y., Chao, C., Liu, J., et al., 2018. Classification and sedimentary characteristics of lacustrine hyperpycnal channels: triassic outcrops in the south Ordos basin, central China. Sediment. Geol. 368, 68–82.
Xu, X.F., Wen, C.J., Li, Y.P., Ren, Z.Y., Xiao, D.S., Feng, Y.Q., 2017. Characteristics and formation conditions of tight tuff reservoir of Tiaohu Formation in Malang Depression. Lithologic Reservoirs 29 (3), 34–41 (in Chinese with English abstract).
Yang, S., Hu, W., Wang, X., et al., 2019. Duration, evolution, and implications of volcanic activity across the Ordovician–Silurian transition in the Lower Yangtze region, South China. Earth Planet Sci. Lett. 518, 13–25.
Yang, W., Xue, L.H., Tang, J., 2015. Analysis and evaluation of different measuring methods for shale porosity. Acta Sedimentol. Sin. 33, 1258–1264.
Yao, Y., Liu, D., Che, Y., Tang, D., Tang, S., Huang, W., 2010. Petrophysical characterization of coals by low-field nuclear magnetic resonance (NMR). Fuel 89 (7), 1371–1380. https://doi.org/10.1016/j.fuel.2009.11.005.
Zhang, G.Y., Zou, C.N., Zhu, R.K., Yuan, X.J., Zhao, X., 2010. Petroleum geology and exploration for volcanic reservoirs in the sedimentary basins of China. Strategic Study of CAE 12 (5), 30–38 (in Chinese with English abstract).
Zhang, W., Yang, W., Xie, L., 2017. Controls on organic matter accumulation in the Triassic chang 7 lacustrine shale of the Ordos basin, central China. Int. J. Coal Geol. 183, 38–51.
Zhang, W.Z., Yang, H., Peng, P.A., et al., 2009. The influence of Late Triassic volcanism on the development of Chang 7 high grade hydrocarbon source rock in Ordos Basin. Geochimica 38 (6), 573–582.
Zhang, Z., Xu, G., Yuan, H., Wang, C., Fan, L., 2013. Characteristics and controlling factors of Carboniferous volcanic reservoir in Hashan area, Junggar Basin. Journal of Northeast Petroleum University 37 (4), 39–46.
Zhao, H., Huang, W., Wang, C., Di, Y., Qi, J., Xiao, Y., Liu, J., 2009. Micropores from devitrification in volcanic rocks and their contribution to reservoirs. Oil Gas Geol. 30, 47–58 (in Chinese with English abstract).
Zheng, H., Sun, X., Wang, J., Zhu, D., Zhang, X., 2018b. Devitrification pores and their contribution to volcanic reservoirs: a case study in the Hailar Basin, NE China. Mar. Petrol. Geol. 98, 718–732.
Zheng, H., Sun, X., Zhu, D., Tian, J., Wang, P., Zhang, X., 2018a. Characteristics and factors controlling reservoir space in the Cretaceous volcanic rocks of the Hailar Basin, NE China. Mar. Petrol. Geol. 91, 749–763.
Zhong, R., Sun, S.P., Fu, Z.M., 1996. Volcanic event deposits and stratigraphic correlation of the late Carboniferous-Early Permian in Shandong and adjacent regions.Acta. Geologica Sinica 70 (2), 142–152 (in Chinese with English abstract).
Zhu, S., Cui, H., Jia, Y., Zhu, X., Ma, L., 2019. Occurrence, composition, and origin of analcime in sedimentary rocks of non-marine petroliferous basins in China. Mar. Petrol. Geol. 113, 104164.
Zou, C.N., 2011. Unconventional Petroleum Geology (In Chinese): Beijing, China. Geological Publishing House, p. 306.